Eur. Phys. J. C (2026) 86:564
https://doi.org/10.1140/epjc/s10052-026-15806-w

THE EUROPEAN PHYSICAL JOURNAL C

Regular Article - Theoretical Physics

Evidence for evolving dark energy from DESI DR2 BAO and Pantheon$^+$, DES-Dovekie, and Union3

Himanshu Chaudhary[1,2,a], **Salvatore Capozziello**[3,4,5,b], **Vipin Kumar Sharma**[6,c], **Isidro Gómez-Vargas**[7,d], **G. Mustafa**[8,9,e]

[1] Department of Physics, Babeş-Bolyai University, Kogălniceanu Street, Cluj-Napoca 400084, Romania
[2] Research Center of Astrophysics and Cosmology, Khazar University, 41 Mehseti Street, Baku AZ1096, Azerbaijan
[3] Dipartimento di Fisica "E. Pancini", Università di Napoli "Federico II", Complesso Universitario di Monte Sant' Angelo, Edificio G, Via Cinthia, Napoli 80126, Italy
[4] Istituto Nazionale di Fisica Nucleare (INFN), sez. di Napoli, Via Cinthia 9, Napoli 80126, Italy
[5] Scuola Superiore Meridionale, Via Mezzocannone 4, Napoli 80134, Italy
[6] International Center for High Energy Physics and Applications, Lovely Professional University, Phagwara, Punjab 144411, India
[7] Department of Astronomy, University of Geneva, Chemin Pegasi 51, Versoix, Geneva 1290, Switzerland
[8] Department of Physics, Zhejiang Normal University, Jinhua 321004, People's Republic of China
[9] College of Graduate Studies, Walailak University, Thasala, Nakhon Si Thammarat 80160, Thailand

Received: 3 March 2026 / Accepted: 2 May 2026

Abstract Evidences for evolving dark energy are shown using baryon acoustic oscillation measurements from the recent Dark Energy Spectroscopic Instrument Data Release 2, combined with different Type Ia supernova datasets (Pantheon$^+$, DES-Dovekie, and Union3) and the CMB compressed likelihood. We examine several dark energy parameterizations, including the Logarithmic, Exponential, CPL, BA, JBP, Thawing, Mirage, and GEDE models. Analyzing the DESI DR2 measurements alone, we find that evidence for evolving dark energy is primarily driven by the LRG1-2 tracers, as their inclusion yields a preferred value of $w_0 > -1$. However, as each tracer provides only limited observables, this preference can result in an underconstrained and potentially unstable inference. Further, we find that each dark energy model predicts values in the $w_0 > -1$, $w_a < 0$ quadrant, a region characterized by the Quintom-B type dark energy scenario. The logarithmic bayes factor shows that, among all models, the Mirage model shows the inconclusive-to-moderate evidence across all dataset combinations. Consistently, the statistical significance remains modest, with $N\sigma \sim$ 1.1-2.3, and no model showing a robust preference for dynamical dark energy using late-time datasets alone. The evolution of $w(z)$ shows a phantom crossing around $z \sim 0.5$ in most dynamical dark energy models, and the evolution of $f_{\rm DE}(z)$ converges to $f_{\rm DE}(0) = 1$ in all dark energy models.

1 Introduction

Dark energy (DE) has been postulated to account for the observed accelerated expansion of the Universe [1,2]. The advent of a new era of precision cosmology has been made possible by recent developments in large-scale structure surveys, which have allowed for rigorous testing of the conventional positive cosmological constant with cold dark matter, i.e., ΛCDM paradigm [3]. Among these, the Dark Energy Spectroscopic Instrument (DESI) is notable for its use of Baryon acoustic oscillations (BAO) observations to track cosmic expansion [4–9]. By analyzing standard cosmological rulers such as BAO, it is possible to place constraints on whether DE operates as a cosmological constant or exhibits time-dependent dynamical behavior [10–15].

Planck's first-year data release in 2013 [16] indicated $w = -1.13^{+0.13}_{-0.14}$, slightly favoring the phantom regime. Subsequent improvements in supernova calibration through the 2014 Joint Light-curve Analysis (JLA) dataset [17] alleviated this tension, and combining JLA with Planck2013 results brought dark energy constraints into agreement with ΛCDM. The Planck-15 analysis [18,18], which adopted JLA as its default supernova dataset, confirmed this consistency, reporting $w = -1.006^{+0.085}_{-0.091}$. More recently, the 2022 Pantheon$^+$

[a] e-mail: himanshu.chaudhary@ubbcluj.ro
himanshuch1729@gmail.com
[b] e-mail: capozziello@na.infn.it
[c] e-mail: vipin.339122@lpu.co.in
[d] e-mail: isidro.gomezvargas@unige.ch
[e] e-mail: gmustafa3828@gmail.com (corresponding author)

Published online: 22 May 2026

compilation [19] found $w = -0.90 \pm 0.14$ from supernova data alone, and $w = -0.978^{+0.024}_{-0.031}$ when combined with CMB and BAO measurements. While these results remain consistent with ΛCDM within 2σ, they show a mild deviation relative to earlier datasets. This trend is reinforced by the Union3 compilation [20], which reports a mild 1.7–2.6σ tension with ΛCDM, favoring models where $\omega_0 > -1$ and $\omega_a < 0$. Collectively, these observations point toward a potentially evolving dark energy component, with an equation of state that increases over time and a present value $w > -1$.

In 2024, building on hints of the evolving nature of dark energy from the Pantheon$^+$ and Union3 compilations, DES-SN5YR found that whether using supernova data alone or in joint fits with the CMB, BAO, and three two point (3×2pt) measurements which refer to the joint analysis of three two-point correlation functions: galaxy clustering, galaxy–galaxy lensing, and cosmic shear, the best fit equation of state (EoS w is consistently slightly greater than -1 at more than the 1σ level. This behavior agrees with results from Union3 and supports a trend toward mildly dynamical dark energy. In the same year, DESI released its first year BAO data [5]; When combined with CMB, Pantheon$^+$, Union3, and DES-SN5YR, these measurements yield (w_0, w_a) constraints that depart from ΛCDM at the levels 2.6σ, 2.5σ, 3.5σ, and 3.9σ, respectively. DESI DR2 BAO measurements [7], when combined with data from CMB only, exclude ΛCDM with a significance of 3.1σ. Including additional supernova data sets Pantheon$^+$, Union3, and DES SN5YR yields exclusion significances of 2.8σ, 3.8σ, and 4.2σ, respectively. Recently, the DES Collaboration reported improved cosmological constraints from a re-analysis of the DES-SN5YR catalog, showing that the preference for dynamical dark energy is reduced to a statistical significance of 3.2σ, compared to the earlier 4.2σ result obtained with DES-SN5YR [21]. Yet several studies have also shown that, in the DES-SN5YR dataset, the evidence for dynamical dark energy is biased by low-redshift SNe Ia [22–25]. Compared to DR1, DR2 offers tighter constraints with improved precision and reduced uncertainties. Following the DR2 BAO release, [8,9] performed an extended analysis of dark energy dynamics and confirmed evidence of a time-varying EoS. Evidence for a time-evolving dark energy model with a statistical significance exceeding 5σ has also been reported [26].

The high-precision BAO measurements from the DESI LRG1 sample, which span redshifts of approximately $z \approx 0.4$–0.6, probe epochs within the DE dominated era. As such, these LRG datasets are particularly sensitive to the signatures of cosmic acceleration, making them valuable for testing time-dependent DE models [27,28]. Numerous studies have reported hints of dynamical dark energy using DESI measurements, supporting the possibility of deviations from the ΛCDM model [29–52]. In parallel, model-independent and non-parametric approaches have been developed to reconstruct the expansion history without assuming a specific form for $w(z)$ [53–58]. Alongside these efforts, alternative theoretical frameworks including holographic dark energy, ricci dark energy, non-cold dark matter, exotic dark matter scenarios, braneworld models and monodromic dark energy have also been explored in light of the DESI measurements [59–64]. In particular, quintessence-based interpretations of evolving dark energy in light of DESI DR2 have been widely explored, with scalar-field dynamics [65–73]. In addition, modified theories of gravity have been investigated using the DESI measurements [74,75], while potential tensions between DESI DR2 and CMB observations have also been examined [76]. The role of topological effects in shaping the behavior of dynamical dark energy has likewise been explored [77]. In a related direction, several studies have also investigated the impact of $\sum m_\nu$ in the context of DESI DR1/DR2 using extended twelve-parameter dynamical dark energy models and late-time dark energy scenarios. [78–81]. Indeed, these developments have also raised questions about the status of the H_0 tension in light of DESI measurements, which suggest evidence for dynamical dark energy and may point toward the need for new physics to resolve this discrepancy [82–85]

Motivated by the above studies, in this paper we explore several dark energy models beyond the CPL parametrization, focusing exclusively on late-time datasets. In particular, we compare phenomenological constraints on the dark energy equation of state w derived with and without DESI LRG1 data. We further extend this analysis by incorporating different SNe Ia samples together with DESI DR2 and compressed CMB likelihoods. This approach allows us to assess the statistical significance of dynamical dark energy features and to isolate the role of late-time observations in driving the inferred evolution. Our paper is organized as follows. In Sect. 2, we introduce the cosmological background equations and models. Section 3 details the core of this work with datasets and methodology using the Markov Chain Monte Carlo (MCMC) sampling against the publicly available DESI DR2 data, while Sect. 4 is dedicated to the discussion of results. In Sect. 5, we draw the conclusions.

2 Background equations and dark energy models

Assuming a spatially flat Friedmann-Lemaître-Robertson-Walker (FLRW) cosmological background

$$ds^2 = -dt^2 + a^2(t)[dr^2 + r^2(d\theta^2 + \sin^2\theta d\phi^2)], \quad (1)$$

where $a(t)$ is the time-dependent cosmological scale factor and (r,θ,ϕ) are the standard spherical coordinates, and considering the late-time Universe – specifically, where radiation can be neglected – the first Friedmann equation arising from

the Einstein field equations

$$G_{\mu\nu} = 8\pi G\, T^{(m)}_{\mu\nu}, \tag{2}$$

takes the form:

$$H^2 = \frac{8\pi G}{3}\left(\rho_{\rm m} a^{-3} + \rho_{\rm de}\right). \tag{3}$$

where $T^{(m)}_{\mu\nu}$ is the standard matter-energy component, $G_{\mu\nu} = R_{\mu\nu} - g_{\mu\nu}R/2$ is the Einstein tensor, and G is the Newtonian gravitational constant. The continuity equation in FLRW background reads

$$\dot{\rho}_{\rm x} + 3H(1 + w_{\rm x})\rho_{\rm x} = 0, \tag{4}$$

where $\rho_{\rm x}$ represents the energy density of each component with x$\in$ (matter, DE), over $\dot{()}$ represents the cosmic time derivative, and w_x represents the equation of state parameter (EoS).

The expansion history of the Universe is governed by the dimensionless Hubble parameter $E(z) = \dfrac{H(z)}{H_0}$, where $H(z) = \dfrac{\dot{a}}{a}$ is the Hubble parameter in function of the redshift z, and H_0 is its present-day value i.e., at $z = 0$. Using Eq. (3), the functional $E(z)^2$ is given by:

$$E(z)^2 = \Omega_m(1+z)^3 + \Omega_r(1+z)^4 + \Omega_\Lambda f_{\rm DE}(z), \tag{5}$$

where Ω_m, Ω_r, and Ω_Λ are the present-day fractional densities of matter, radiation, and dark energy, respectively. Also, here f_{DE} represents the evolution of DE [86,87]. The evolution of DE ($\rho_{\rm de}$) within Eq. (3) will be the following solution of Eq. (4):

$$f_{\rm DE}(z) \equiv \frac{\rho_{\rm DE}(z)}{\rho_{\rm DE,0}} = \exp\left[3\int_0^z \frac{1 + w(z')}{1 + z'}\, dz'\right] \tag{6}$$

where $\rho_{\rm de,0}$ is the present value of the DE density. For the constant w, the (6) simply $(1+z)^{3(1+w)}$, and a cosmological constant corresponds to $w = -1$. We also consider the Mirage Dark Energy parametrization [88], constructed to reproduce the CMB distance to last scattering of ΛCDM while allowing a dynamical equation of state $w(a) = w_0 + w_a(1-a)$. It effectively yields $w \approx -1$ near the pivot scale factor $a \approx 0.7$. In this framework, the CPL parameters satisfy $w_a = -3.66\,(1 + w_0)$, and the Thawing Dark Energy parametrization, which satisfies $w_a = -1.58\,(1 + w_0)$. Apart from this, we also consider different dynamical dark energy models; see Table 1, where we present the corresponding EoS and $f_{\rm DE}(z)$ for those models.

Although no fundamental principle uniquely specifies the optimal functional form for parameterisations, observational data can be employed to constrain and select those formulations that are both cosmologically consistent and phenomenologically viable. In the following, we examine several distinct parameterisation schemes for describing the evolution of dark energy (DE).

3 Dataset and methodology

To constrain the free parameters of each DE model considered in this work, we use the cosmological inference code `SimpleMC`. In our analyses, we use dynamic nested sampling [97,98] using the `dynesty` Python package [99], as implemented within `SimpleMC`. To determine the number of live points, we follow the general rule of using $50 \times n_{\rm dim}$, where $n_{\rm dim}$ denotes the number of free parameters of the corresponding DE model.

We use the Bayesian evidence selection criterion to assess whether the DE models are statistically preferred over the ΛCDM model. The Bayesian evidence, Z, is defined as the integral of the likelihood over the prior volume, $Z = \int_\Omega \mathcal{L}(\theta)\,\pi(\theta)\,d\theta$, where $\mathcal{L}(\theta) \equiv P(D|\theta, M)$ is the likelihood of the data D given the parameters θ and model M, and $\pi(\theta) \equiv P(\theta|M)$ is the prior distribution of the parameters within that model. To compare two competing models, we compute the Bayes factor in logarithmic form, $\ln \mathcal{B}_{ij} = \ln \mathcal{Z}_i - \ln \mathcal{Z}_j$, where $\ln \mathcal{Z}_i$ and $\ln \mathcal{Z}_j$ denote the Bayesian evidences of models i and j, respectively. In our case, we report the Bayes factors $\ln \mathcal{B}_{ij}$ for the dynamical DE models relative to the ΛCDM model, based on the current observational data. Here, i denotes the dynamical DE model, while j denotes the ΛCDM model. Consequently, $\ln \mathcal{B}_{ij} > 0$ (< 0) indicates a preference for the DDE model (ΛCDM). The strength of model preference is interpreted using the Jeffreys scale [100]: values of $\ln \mathcal{B}_{ij} < 1$ are considered inconclusive; $1 \le \ln \mathcal{B}_{ij} < 2.5$ indicate weak evidence; $2.5 \le \ln \mathcal{B}_{ij} < 5$ correspond to moderate evidence; $5 \le \ln \mathcal{B}_{ij} < 10$ signify strong evidence; and $\ln \mathcal{B}_{ij} \ge 10$ is regarded as decisive evidence. In our analysis, the Bayesian evidence is computed by the `dynesty` package by algorithm.

The obtained results are subsequently analyzed and visualized using the `GetDist` package [101]. Our analysis is based on data obtained from Baryon Acoustic Oscillation measurements, Type Ia supernovae, and Compressed CMB likelihood, which are detailed below:

- *Baryon Acoustic Oscillation:* In our analysis, we use the recent BAO measurements from DESI Data Release 2 (DR2) [7]. These measurements are extracted using various tracers such as the Bright Galaxy Sample (BGS),

https://github.com/ja-vazquez/SimpleMC.git

Table 1 Dark energy parameterizations with their equations of state $w(z)$ and evolution functions $f_{DE}(z)$

Parameterization	$w(z)$	$f_{DE}(z)$	Reference
Logarithmic	$w_0 + w_a \log(1+z)$	$(1+z)^{3(1+w_0)} e^{\frac{3}{2} w_a (\log(1+z))^2}$	[89,90]
Exponential	$w_0 + w_a \left[\frac{z}{1+z} + \frac{1}{2} \left(\frac{z}{1+z} \right)^2 \right]$.	$e^{\left[3w_a\left(\frac{-z}{1+z}\right)\right]} (1+z)^{3(1+w_0+w_a)} e^{\left[3w_a\left(\frac{1}{4(1+z)^2} + \frac{1}{2(1+z)} - \frac{3}{4}\right)\right]} (1+z)^{\frac{3}{2} w_a}$	[91]
CPL	$w_0 + \frac{z}{1+z} w_a$	$(1+z)^{3(1+w_0+w_a)} e^{-\frac{3w_a z}{1+z}}$	[92,93]
BA	$w_0 + \frac{z(1+z)}{1+z^2} w_a$	$(1+z)^{3(1+w_0)} (1+z^2)^{\frac{3w_a}{2}}$	[94]
JBP	$w_0 + \frac{z}{(1+z)^2} w_a$	$(1+z)^{3(1+w_0)} e^{\frac{3w_a z^2}{2(1+z)^2}}$	[95]
GEDE	$-1 - \frac{\Delta}{3\ln(10)} \left[1 + \tanh\left(\Delta \log_{10}\left(\frac{1+z}{1+z_t} \right) \right) \right]$	$\left(\frac{1-\tanh\left(\Delta \log_{10}\left(\frac{1+z}{1+z_t} \right) \right)}{1+\tanh\left(\Delta \log_{10}(1+z_t) \right)} \right)$	[96]

Luminous Red Galaxies (LRG1–3), Emission Line Galaxies (ELG1–2), Quasars (QSO), and Lyman-α forests. To incorporate these measurements, one must compute the Hubble distance $D_H(z) = \frac{c}{H(z)}$, the comoving angular diameter distance $D_M(z) = c \int_0^z \frac{dz'}{H(z')}$, and the volume-averaged distance $D_V(z) = \left[z, D_M^2(z), D_H(z) \right]^{1/3}$. It is necessary to derive the following ratios: D_M/r_d, D_H/r_d, D_V/r_d, and D_M/D_H to constrain the parameters of each model, where r_d is the sound horizon. In flat ΛCDM, it is $r_d = 147.09 \pm 0.2$ Mpc [102].

- *Type Ia supernovae:* We also use three different SNe Ia compilations to improve the constraints on cosmological parameters. Among them, the Pantheon$^+$ (PP) sample [19] includes 1701 light curves from 1550 SNe Ia observations spanning the redshift range $0.01 \leq z \leq 2.26$. We exclude light curves at $z < 0.01$, as such low redshift data are affected by significant systematic uncertainties due to peculiar velocities. We also use the re-calibrated 1,820 photometric light curves collected over five years by the Dark Energy Survey Supernova Program (DES-Dovekie) [21], which includes 1,623 DES-discovered Type Ia supernovae and 197 externally sourced low-z supernovae from the CfA and CSP samples [103–105]. The revised DES-Dovekie has 1718 SNe Ia overlapping between DES-Dovekie and DES-SN5YR [106], and Union3 compilation of 2087 cosmologically useful SNe Ia from 24 datasets over a redshift range from $0.050 \leq z \leq 2.26$ [20]. In our analysis, we marginalize over $\mathcal{M}$ parameter; for further details, see Equations (A9–A12) of [107].
- *Compressed CMB likelihood:* Finally, we use the compressed CMB likelihood because the dynamical dark energy models considered affect only the late-time expansion history of the Universe and mainly modify the geometrical features of the CMB. The full CMB spectrum includes small non-geometrical anomalies, such as the lensing amplitude and the low-ℓ power deficit, which may reflect residual systematics and bias dark energy estimates. For example, Planck data alone show a $\gtrsim 2\sigma$ preference for phantom dark energy [108], mostly due to the lack of large-scale power. To avoid such biases, we rely on the compressed CMB likelihood. We use the CMB information compressed into the three parameters $\{ \theta_\star, \omega_b, \omega_{cb} \}$, which is modeled as a 3×3 Gaussian likelihood [7] (see Appendix A, Eqs. A1 and A2).

Table 2 The table shows the parameters and the priors used in our analysis for each DE model. The symbol $\mathcal{U}$ denotes that we use uniform priors

Parametrization	Parameter	Prior
ΛCDM	H_0	$\mathcal{U}[40, 90]$
	$\Omega_b h^2$	$\mathcal{U}[0.02, 0.025]$
	Ω_m	$\mathcal{U}[0.1, 0.5]$
Dark energy	w or w_0	$\mathcal{U}[-3, 1]$
	w_a	$\mathcal{U}[-3, 2]$
Thawing/Mirage	w_0	$\mathcal{U}[-3, 1]$
Emergent	Δ	$\mathcal{U}[-3, 10]$

In this analysis, the radiation density parameter is defined as $\Omega_r = 2.469 \times 10^{-5} h^{-2} (1 + 0.2271 N_{\rm eff})$ [109], where $N_{\rm eff} = 3.04$ represents the standard effective number of relativistic species. The dark energy density parameter is determined from the flatness condition, $\Omega_\Lambda = 1 - \Omega_r - \Omega_m$, so that both Ω_r and Ω_Λ are computed from the remaining cosmological parameters. In this analysis, we use several DE models, with the chosen priors summarized in Table 1

4 Results

In this section, we explore various DE parameterizations to show the evidence for evolving DE. From this perspective, we first consider the DESI DR2 measurements alone to identify

what drives the evolving nature of DE in this dataset. We then combine the DESI DR2 data with different Type Ia supernova (SNe Ia) measurements (Pantheon$^+$, DES-Dovekie, Union3) and a CMB compressed likelihood. Next, we compute the Bayes factor in logarithmic space $\ln \mathcal{B}_{i,j}$ to assess which model performs best among the models considered. Finally, we plot the evolution of the equation of state (w) and the normalized ($f_{\rm DE}$) as functions of redshift.

4.1 Evidence for evolving dark energy in DESI BAO biased by LRG1 and LRG2 tracers

Motivated by Fig. 1, the LRG1 ($z_{\rm eff} = 0.510$) and LRG3+ELG1 ($z_{\rm eff} = 0.934$) BAO points appear in tension with the Planck ΛCDM value $\Omega_m = 0.315 \pm 0.007$, at about 2.42σ and 2.60σ, respectively. This trend becomes more prominent when comparing the value of Ω_m at $z_{\rm eff} = 0.510$ and $z_{\rm eff} = 0.934$ from the LRG1 and LRG3+ELG1 datasets, which are in tension with various supernovae compilations, showing discrepancies of 2.06σ, 1.67σ, and 1.80σ for LRG1 and 2.24σ, 2.51σ, and 2.96σ for LRG3+ELG1 with Pantheon$^+$, Union3, and DES-SN5YR, respectively. These supernova datasets typically have similarly low effective redshifts around $z_{\rm eff} \sim 0.3$. See Table 1 and Sect. 4 of [51] for details.

This behavior is not new, as similar trends have been observed in previous studies. [110] (see Table 1 and Fig. 5) report the LRG1 discrepancy using the DESI DR1 compilation, and note that in DESI DR1 the LRG2 point also exhibits a significant discrepancy. Similar discrepancies are found in [111] using SDSS-IV data (see Table 3 and Fig. 5). More recently, using DESI DR2, [39,51] show that the LRG1 ($z_{\rm eff} = 0.510$) discrepancy persists, and that a comparable tension is also present for LRG3+ELG1 ($z_{\rm eff} = 0.934$).

Indeed, recent work by [112] has explicitly investigated the role of individual DESI tracers in driving the preference for dynamical dark energy. In particular, they show that removing the LRG1 and LRG2 data points significantly affects the inferred constraints on dark energy parametrizations, indicating that these low-redshift tracers play a disproportionate role in driving deviations from ΛCDM. This provides further motivation for treating LRG1 and LRG2 on the same footing in our analysis.

In Fig. 2, considering next information from high-redshift bins alone shows a tension of about 1.84σ, indicating that Ω_m differs between different redshift bins. A similar trend can be observed in the DESI DR1 data, where [110] reports a tension of about 2.20σ when considering next information from high-redshift bins alone. In fact, DESI DR1 shows some improvement; see Table 2 of [51,110] for more details. These findings lead us to investigate the DESI DR2 data beyond the ΛCDM paradigm. In this study, we extend our analysis beyond the ΛCDM model and consider several DE models to investigate the effects of DESI BAO tracers beyond ΛCDM.

Unlike previous studies, our analysis is based on the DESI DR2 dataset and explores a broader class of dark energy parametrizations, including both phenomenological (w_0–w_a) models and physically motivated scenarios such as GEDE. We also perform a systematic comparison by removing LRG1 and LRG2 both individually and jointly, allowing us to directly quantify their impact on the inferred dark energy evolution

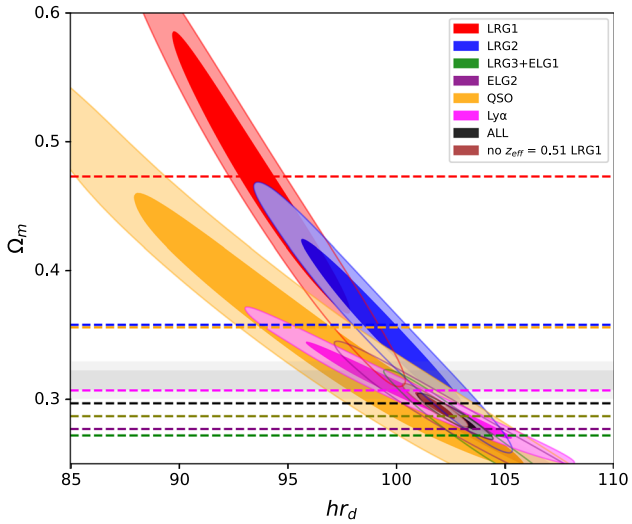

Fig. 1 The figure shows the posterior distributions at the 1σ and 2σ confidence levels in the $\Omega_m - hr_d$ contour plane for different tracers corresponding to various $z_{\rm eff}$ values from the DESI DR2 dataset within the ΛCDM model. The horizontal lines correspond to the mean values of Ω_m for each tracer, and the gray band represents the Planck ΛCDM prediction for $\Omega_m = 0.315 \pm 0.007$

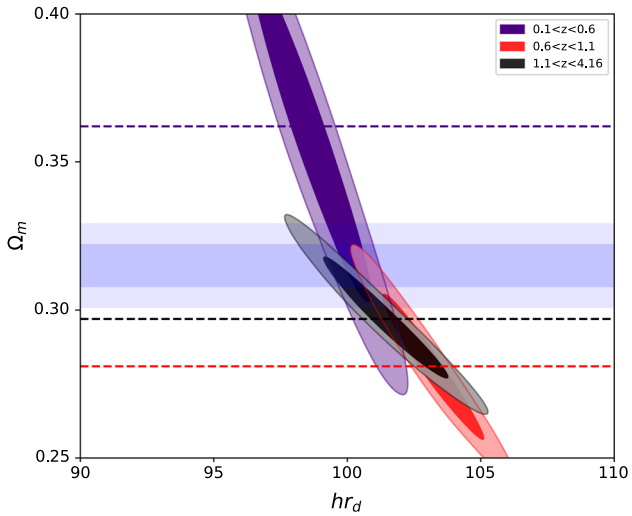

Fig. 2 The figure shows the posterior distributions in the $\Omega_m - hr_d$ plane using different redshift bins from the DESI DR2 compilation. The blue band represents the Planck ΛCDM prediction for Ω_m

In Fig. 3 shows the triangle plot of the different DE models using the DESI DR2 measurements (excluding the BGS datapoint), for no LRG1, no LRG2, no LRG1 & LRG2, and the full DESI DR2 sample. The diagonal panels show the 1D marginalized posterior distributions for each parameter. The off-diagonal panels show the 2D marginalized confidence contours at 68% and 95% intervals. Table 3 shows the numerical values obtained for each model using MCMC analysis.

Figure 3a shows the constraints on the wCDM model. When the LRG1 and LRG2 datasets are included, the inferred w deviates from the ΛCDM prediction ($w = -1$). Conversely, removing LRG1 and LRG2 fully restores the ΛCDM concordance.

Figure 3b–f show the constraints on the Logarithmic, Exponential, CPL, BA, and JBP redshift parameterizations. In each case, it can be observed that when the LRG1 and LRG2 data points are included alternately in the analysis, the predicted value $w_0 > -1$ shows a deviation from the ($w_0 = -1, w_a = 0$) corresponds to the ΛCDM model in $w_0 - w_a$ plane, and it can be observed that ω_a also shifts to large negative values, extending beyond the previous limits to accommodate $w_0 > -1$. This suggests that the evolving DE in the DESI DR2 data could be driven by the LRG1 and LRG2 datapoints, particularly at low redshift ($z \lesssim 0.3$). This behavior is consistent with the findings of [112], where the removal of LRG1 and LRG2 similarly reduces the apparent preference for dynamical dark energy, reinforcing the interpretation that these tracers play a key role in driving the signal.

Figure 3g and h show the constraints on the Calibrated Thawing and Calibrated Mirage models using DESI DR2 measurements. Similar effects of the LRG1 and LRG2 datapoints are observed for ω_0: when LRG1 and LRG2 are included alternately, the inferred value satisfies $w_0 > -1$,which in turn drives $w_a < 0$. For the Mirage model, we again find $w_0 > -1$ and, consequently, $w_a < 0$.

Figure 3i shows the constraints on the GEDE model. Similar effects of the LRG1 and LRG2 datapoints are also observed here: when the LRG1 and LRG2 datapoints are included alternately, the model predicts $\Delta = -1.010$, which lies far from the ΛCDM point ($\Delta = 0$). In contrast, without the LRG1 and LRG2 datapoints, GEDE predicts $\Delta = -0.300$, much closer to ΛCDM. In both cases, the negative value of Δ indicates an injection of energy at earlier redshifts. These results highlight that the LRG1 and LRG2 tracers play a crucial role in driving the preference for dynamical dark energy in the DESI DR2 BAO dataset.

In addition to the effects of the LRG1-2 tracers, an interesting feature is also evident: a negative correlation between Ω_m and hr_d. This anti-correlation has been observed previously in several independent analyses. Specifically, [113,114] have reported this trend using Observational Hubble Data (OHD); [111,113,115–121] using Type Ia supernovae (SNe Ia); [113,122] by combining OHD and SNe Ia; [123,124] using Gamma-Ray Bursts (GRBs); [111,113,125–130] using standardizable QSOs; and similar patterns have been discussed in studies of strong-lensing time delays in lensed QSOs [131–133] and lensed SNe Ia [134,135].

It is worth noting that each tracer provides only a limited set of observables, such as D_H/r_d and D_M/r_d, while the fitted models involve a larger number of parameters. This can lead to an underconstrained setup, increasing the risk of overfitting and posterior instability, particularly when individual redshift bins are analyzed. As a result, the apparent anomaly in Ω_m may reflect statistical artifacts rather than genuine physical constraints. Motivated by this, we go beyond the DESI BAO-only analysis in the following sections by incorporating different Type Ia supernova samples and a CMB compressed likelihood.

4.2 Evidence for evolving dark energy using DESI DR2 BAO with other datasets

In the previous section, we constrained each DE model using only the DESI DR2 dataset. We found that, across all models, the posterior distributions in the w_0–w_a plane indicate that w_a remains poorly constrained when relying solely on DESI DR2 data. To improve these constraints and break parameter degeneracies, we now incorporate additional datasets, combining DESI DR2 with various Type Ia supernova compilations and CMB measurements.

Table 4 presents the numerical values obtained for each cosmological model using MCMC analysis. Here, we compared the predicted values of the Hubble parameter h and the matter density Ω_m from each model with the ΛCDM model using CMB + DESI DR2 data, both alone and in combination with Type Ia supernova datasets (Pantheon$^+$, DES-Dovekie, Union3). Using ΛCDM as the reference model, we find that most DE parameterizations show weak evidence in both h and Ω_m. In particular, the wCDM, Thawing, Mirage, and GEDE models show deviations that remain below the 1σ level across all dataset combinations, indicating consistency with the ΛCDM predictions. For the CPL, BA, and JBP parameterizations, the deviations in h and Ω_m increase but remain below the 2σ level for all datasets. The largest deviations are observed in the Logarithmic and Exponential models, where tensions in both parameters approach or exceed the 2σ level for certain dataset combinations.

In Fig. 4, we show the inferred values of the Hubble parameter h for each cosmological model. It can be observed that none of the dark energy models alleviate the Hubble tension, as their inferred h values remain below the *Riess* predictions [136,137] but consistent with the *Planck* predictions [102]. This can be understood in two ways. First, dynamical dark energy models cannot reduce the sound horizon since

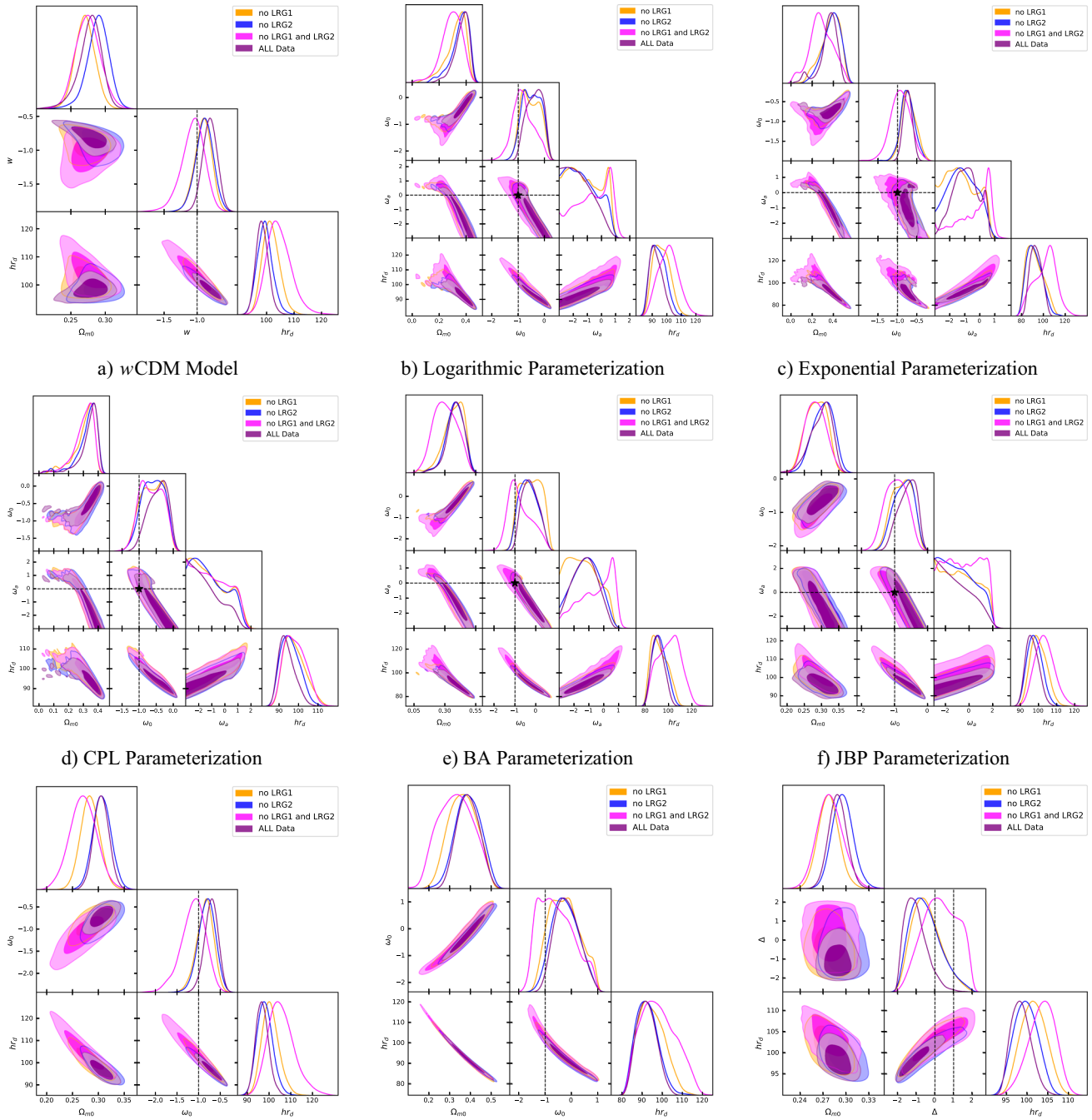

a) wCDM Model b) Logarithmic Parameterization c) Exponential Parameterization

d) CPL Parameterization e) BA Parameterization f) JBP Parameterization

g) Thawing Parameterization h) Mirage Parameterization i) GEDE Parameterization

Fig. 3 The figure shows the posterior distributions wCDM, Logarithmic, Exponential, CPL, BA, JBP, Thawing, Mirage, and GEDE models at 68% (1σ) and 95% (2σ) confidence, using no LRG1, no LRG2, no LRG1 and LRG2, and the full DESI DR2 sample

dark energy is sub-dominant at recombination. Therefore, if these models attempt to increase the inferred value of h, they become inconsistent with BAO measurements. Second, in all dynamical dark energy models predicting $w > -1$, the dark energy density scales as $f_{\rm DE} > 1$, leaving $\Omega_m h^2$ nearly unchanged from the ΛCDM prediction. To maintain consistency with the observed $H(z)$ data, a larger $f_{\rm DE}$ requires a lower inferred H_0, thereby intensifying the tension. Similar behavior has been reported in [39,138], where the CPL model also favors $w_0 > -1$, leading to a reduced H_0 when DESI DR2 is combined with CMB and SNe Ia data.

Now we turn to the main observation of this paper. In Fig. 5, we present the relevant parameter planes. Specifically, Fig. 5a shows the $\Omega_m - w_0$ plane for the wCDM

model. Our results, based on the combination of DESI DR2 and CMB data, are consistent with the findings of [7] ($w = -1.005 \pm 0.036$). Furthermore, our results also agree with the constraints obtained from DESI DR2 combined with CMB data and various SNe Ia measurements, as reported by [7]: $w = -0.986 \pm 0.026$ with PP, $w = -0.983 \pm 0.024$ with DES-Dovekie, and $w = -0.979 \pm 0.031$ with Union3.

Figure 5b–f show the w_0-w_a plane for the Logarithmic, Exponential, CPL, BA, and JBP redshift parameterizations, respectively. In each (w_0, w_a) plane, the point $(w_0 = -1, w_a = 0)$ corresponds to the ΛCDM model. It is worth noting that for each DE model, when combining the DESI DR2 measurements with CMB data and different Type Ia supernova datasets, the inferred constraints favor the region $w_0 > -1$ and $w_a < 0$. This quadrant is also characteristic of the Quintom-B scenario, defined by $(w_0 > -1,\ w_a < 0,\ w_0 + w_a < -1)$, in which the equation of state evolves from phantom dark energy to quintessence consistent with previous findings in the literature [139–141].

Figures 5g and h show the $w_0 - \Omega_m$ plane for the calibrated Thawing and Mirage redshift parameterizations. In the case of the calibrated Thawing model, we observe that for each combination of DESI DR2 with the different measurements of SNe Ia and CMB, the value of $w_0 > -1$ results in $w_a < 0$. Similarly, in the case of the calibrated Mirage model, combining DESI DR2 with CMB and each SNe Ia dataset yields results similar to those from the calibrated Thawing model, with $w_0 > -1$ in all cases and, consequently, $w_a < 0$. In Fig. 5i, which shows the $\Delta - \Omega_m$ plane for the GEDE model. It can be seen that the combination of DESI DR2 and CMB data yields $\Delta = 0.13^{+0.26}_{-0.30}$, consistent with the ΛCDM model. However, when different SNe Ia datasets such as Pantheon$^+$, DES-Dovekie, and Union3 are included, the GEDE model predicts a negative value of Δ, indicating an injection of DE at high redshifts. A similar behavior can also be observed in previous studies [8,9].

4.3 Statistical analysis

In Fig. 6, we show the comparative analysis of different cosmological models relative to the baseline ΛCDM model using the Bayes factor in logarithmic space, $\ln \mathcal{B}_{i,j}$. For the CMB + DESI DR2 combination, we find that the wCDM, JBP, and GEDE models show moderate to weak evidence in favour of ΛCDM, while the CPL, Logarithmic, Exponential, BA, and Mirage models show weak to inconclusive evidence relative to ΛCDM, with the Thawing model showing no clear preference. When Pantheon$^+$ data are added to the CMB + DESI DR2 combination, we find that the wCDM, CPL, Logarithmic, Exponential, JBP, BA, and GEDE models show weak to moderate evidence in favour of ΛCDM, whereas the Thawing and Mirage models show weak evidence relative to ΛCDM. Further, for the combination of DES-Dovekie with CMB + DESI DR2, we find that the wCDM, CPL, Logarithmic, Exponential, JBP, BA, and GEDE models show weak to moderate evidence in favour of ΛCDM, while the Thawing and Mirage models show weak to moderate evidence relative to ΛCDM. Finally, when Union3 is combined with CMB + DESI DR2, we find that the wCDM, JBP, and GEDE models show moderate to weak evidence in favour of ΛCDM, while the CPL, Logarithmic, Exponential, BA, Thawing, and Mirage models show weak to moderate evidence relative to ΛCDM.

We also quantify the preference for dynamical dark energy over the ΛCDM model across different data combinations, taking ΛCDM as the reference model. To assess this, we use the difference in the best-fit chi-square values between the DDE models and the ΛCDM scenario. Since ΛCDM is nested within the broader class of DDE models, $\Delta\chi^2_{\rm MAP}$ is expected to follow a χ^2 distribution with k degrees of freedom, corresponding to the number of additional parameters, assuming Gaussian uncertainties. The statistical significance is then expressed as an equivalent Gaussian $N\sigma$. $\mathrm{CDF}_{\chi^2}\left(\Delta\chi^2_{\rm MAP} \,|\, k \text{ dof}\right) = \frac{1}{\sqrt{2\pi}} \int_{-N}^{N} e^{-x^2/2}\, dx$, where k denotes the number of additional parameters in the DDE model relative to ΛCDM.

We find that wCDM shows no significant improvement over ΛCDM, with $N\sigma \approx 0$ for all dataset combinations, reaching at most 0.14σ for DES-Dovekie. For two-parameter models, CPL yields $N\sigma = 1.65$, 1.13, 1.55, and 2.06 for CMB+DESI, Pantheon$^+$, DES-Dovekie, and Union3, respectively. The Logarithmic parametrization gives $N\sigma = 1.59$, 1.34, 1.65, and 2.12, while the Exponential model gives $N\sigma = 1.64$, 1.19, 1.59, and 2.08. The JBP model shows lower values, $N\sigma = 1.10$, 0.83, 1.38, and 1.82. The BA model gives $N\sigma = 1.66$, 1.27, 1.59, and 2.09. For one-parameter extensions, the Thawing model yields $N\sigma = 1.65$, 1.96, 2.10, and 2.22, while the Mirage model gives $N\sigma = 1.73$, 1.98, 2.24, and 2.32, with the highest values obtained for Union3. The GEDE model shows smaller deviations, with $N\sigma = 0.80$, 0.97, 1.11, and 1.07 across the four dataset combinations.

Indeed, in the case of the CPL model, our results can be compared with previous DESI DR1 and DR2 analyses, which reported a preference for dynamical dark energy at the level of 2.6σ, 2.5σ, 3.5σ, and 3.9σ when DESI DR1 is combined with CMB and Pantheon$^+$, Union3, and DESY5 datasets, respectively [5]. Similarly, in DESI DR2, the preference increases to 3.1σ, 2.8σ, 3.8σ, and 4.2σ for the same dataset combinations [7]. In those analyses, the full CMB information is used from the temperature (TT), polarization (EE), and cross (TE) power spectra from *Planck*, using the Commander likelihood for $\ell < 30$ and CamSpec for $\ell \geq 30$ [142,143], together with the combination of *Planck* and ACT DR6 CMB lensing [144–147].

Table 3 This table presents the numerical values obtained using DESI DR2 measurements for the ΛCDM, wCDM, Logarithmic, Exponential, CPL, BA, JBP, Thawing, Mirage, and GEDE models, with and without the inclusion of the LRG1 datapoint at the 68% (1σ) confidence level

Dataset/Models	Ω_{m0}	w or w_0	w_a	Δ	$h\,r_d$
ΛCDM					
No LRG1	0.275 ± 0.013	–	–	–	101.4 ± 1.2
No LRG2	0.296 ± 0.013	–	–	–	103.4 ± 1.3
No LRG1 & LRG2	$0.281^{+0.016}_{-0.019}$	–	–	–	102.8 ± 1.9
DESI DR2	0.289 ± 0.011	–	–	–	102.1 ± 1.0
wCDM					
No LRG1	0.270 ± 0.015	$-0.910^{+0.140}_{-0.110}$	–	–	$101.6^{+2.7}_{-3.3}$
No LRG2	$0.289^{+0.017}_{-0.014}$	$-0.890^{+0.140}_{-0.120}$	–	–	$99.4^{+2.4}_{-3.0}$
No LRG1 & LRG2	0.275 ± 0.018	$-1.07^{+0.190}_{-0.150}$	–	–	$104.6^{+3.6}_{-4.9}$
DESI DR2	$0.277^{+0.019}_{-0.013}$	-0.810 ± 0.110	–	–	$98.4^{+2.1}_{-2.4}$
Logarithmic					
No LRG1	$0.323^{+0.092}_{-0.038}$	-0.530 ± 0.350	-1.20 ± 1.10	–	$96.3^{+4.9}_{-6.5}$
No LRG2	$0.355^{+0.081}_{-0.035}$	-0.480 ± 0.340	$-1.32^{+0.62}_{-1.60}$	–	$94.1^{+4.4}_{-6.1}$
No LRG1 & LRG2	$0.293^{+0.085}_{-0.060}$	$-0.810^{+0.340}_{-0.460}$	$-0.630^{+1.60}_{-0.78}$	–	101.0 ± 7.0
DESI DR2	$0.366^{+0.066}_{-0.033}$	$-0.370^{+0.380}_{-0.280}$	$-1.530^{+0.053}_{-1.400}$	–	$92.7^{+3.4}_{-5.2}$
Exponential					
No LRG1	$0.370^{+0.120}_{-0.061}$	$-0.710^{+0.160}_{-0.200}$	$-1.30^{+1.70}_{-1.50}$	–	$92.1^{+5.5}_{-10.0}$
No LRG2	$0.383^{+0.100}_{-0.066}$	-0.740 ± 0.180	-1.16 ± 0.94	–	$91.6^{+5.7}_{-8.3}$
No LRG1 & LRG2	$0.280^{+0.120}_{-0.100}$	-0.930 ± 0.260	$-0.370^{+1.30}_{-0.57}$	–	$102^{+11.0}_{-9.4}$
DESI DR2	$0.349^{+0.040}_{-0.095}$	-0.740 ± 0.110	$-0.950^{+1.300}_{-0.900}$	–	$93.0^{+4.8}_{-6.0}$
CPL					
No LRG1	$0.303^{+0.083}_{-0.027}$	$-0.620^{+0.410}_{-0.300}$	-1.00 ± 1.30	–	$97.8^{+4.1}_{-6.7}$
No LRG2	$0.325^{+0.080}_{-0.024}$	$-0.590^{+0.370}_{-0.310}$	$-1.10^{+2.00}_{-1.80}$	–	$95.8^{+4.0}_{-5.9}$
No LRG1 & LRG2	0.275 ± 0.065	$-0.950^{+0.340}_{-0.470}$	$-0.270^{+2.00}_{-0.93}$	–	103.4 ± 7.1
DESI DR2	$0.333^{+0.072}_{-0.019}$	$-0.460^{+0.350}_{-0.240}$	$-1.410^{+0.500}_{-1.600}$	–	$94.1^{+3.0}_{-5.1}$
BA					
No LRG1	$0.373^{+0.099}_{-0.055}$	-0.240 ± 0.490	$-1.37^{+0.66}_{-1.40}$	–	$92.2^{+5.3}_{-9.0}$
No LRG2	$0.380^{+0.078}_{-0.061}$	$-0.350^{+0.380}_{-0.520}$	-1.18 ± 0.88	–	$92.1^{+5.2}_{-6.9}$
No LRG1 & LRG2	$0.303^{+0.092}_{-0.110}$	$-0.750^{+0.400}_{-0.710}$	$-0.520^{+1.400}_{-0.760}$	–	100.6 ± 9.7
DESI DR2	$0.383^{+0.075}_{-0.054}$	$-0.270^{+0.350}_{-0.470}$	-1.260 ± 0.810	–	$90.9^{+4.5}_{-6.1}$
JBP					
No LRG1	$0.284^{+0.034}_{-0.029}$	$-0.770^{+0.350}_{-0.300}$	$-0.700^{+1.000}_{-2.200}$	–	$99.9^{+4.0}_{-5.0}$
No LRG2	$0.304^{+0.034}_{-0.027}$	$-0.730^{+0.350}_{-0.270}$	$-0.840^{+0.970}_{-2.100}$	–	$97.8^{+3.7}_{-4.5}$
No LRG1 & LRG2	$0.283^{+0.028}_{-0.032}$	-0.950 ± 0.330	-0.500 ± 1.400	–	$103.2^{+4.8}_{-5.9}$
DESI DR2	$0.297^{+0.038}_{-0.024}$	$-0.620^{+0.340}_{-0.210}$	$-1.050^{+0.710}_{-1.900}$	–	$96.5^{+3.2}_{-4.1}$
Thawing					
No LRG1	0.284 ± 0.018	$-0.850^{+0.210}_{-0.170}$	–	–	$100.7^{+3.4}_{-4.3}$
No LRG2	0.307 ± 0.017	$-0.810^{+0.210}_{-0.180}$	–	–	$98.1^{+3.2}_{-3.9}$
No LRG1 & LRG2	0.271 ± 0.026	$-1.130^{+0.310}_{-0.240}$	–	–	$105.7^{+4.9}_{-6.8}$
DESI DR2	0.306 ± 0.015	$-0.710^{+0.170}_{-0.140}$	–	–	$96.8^{+2.6}_{-3.2}$
Mirage					
No LRG1	0.363 ± 0.066	$-0.260^{+0.480}_{-0.710}$	–	–	$94.4^{+5.7}_{-7.8}$
No LRG2	0.389 ± 0.060	$-0.230^{+0.470}_{-0.560}$	–	–	$92.4^{+4.6}_{-6.3}$

Table 3 continued

Dataset/Models	Ω_{m0}	w or w_0	w_a	Δ	$h\,r_d$
No LRG1 & LRG2	0.328±0.085	$-0.570^{+0.450}_{-0.880}$	–	–	$98.5^{+6.8}_{-11.0}$
DESI DR2	0.389±0.053	$-0.170^{+0.420}_{-0.530}$	–	–	$92.2^{+4.5}_{-5.4}$
GEDE					
No LRG1	0.277±0.014	–	–	$-0.450^{+0.600}_{-0.930}$	101.5±3.0
No LRG2	0.295±0.014	–	–	$-0.500^{+0.570}_{-1.000}$	99.6±2.8
No LRG1 & LRG2	$0.280^{+0.015}_{-0.019}$	–	–	$-0.300^{+1.100}_{-0.890}$	$103.5^{+3.7}_{-2.8}$
DESI DR2	0.289±0.012	–	–	$-1.010^{+0.360}_{-0.750}$	$98.5^{+2.0}_{-2.0}$

[148] also reports evidence for dynamical dark energy in light of DESI DR2, combined with joint ACT [149], SPT [150], and *Planck* data [142,143], for different dark energy parametrizations. In the case of the CPL, JBP, and BA models, previous studies combining DESI DR2 with joint ACT, SPT, and *Planck* likelihoods report significantly higher deviations from ΛCDM. In particular, the CPL model shows $N\sigma = 2.3$-3.9, while the JBP model gives $N\sigma = 2.9$-4.1, and the BA model reaches $N\sigma = 3.0$-4.2, depending on the dataset combination. These values are consistently higher than those obtained in the present analysis, where we find $N\sigma \sim 1.1$-2.1 for the same class of models. In contrast, the present work focuses primarily on late-time measurements, combining DESI DR2 with SNe Ia datasets and compressed CMB likelihoods, with particular emphasis on the preference for dynamical dark energy in the late-time datasets.

4.4 Evolution of the EoS and the energy density function

In this subsection, we show the redshift evolution of the EoS parameter in Fig. 7 and the energy density function in Fig. 8, in order to gain a deeper physical understanding of the models. Figure 7 shows that, for the Logarithmic, Exponential, CPL, BA, JBP, and Mirage models, and for all dataset combinations, $w(z)$ falls below the cosmological constant boundary $w = -1$ at redshifts $z \gtrsim 0.5$, indicating that each model predicts values in the phantom regime ($w < -1$). At lower redshifts, $z \lesssim 0.5$, $w(z)$ rises again above $w = -1$, predicting values in the quintessence-like regime ($w > -1$). This crossing, where $w(z)$ rises from the phantom regime at high redshift to the quintessence-like regime at low redshift by crossing the boundary $w = -1$, is called a *phantom crossing*. This evidence of phantom crossing in our analysis is consistent with previous studies reported in the literature [151–157]. This kind of behavior is characterized by the Quintom-B–type dark energy scenario, and is consistent with previous findings in the literature [139–141]. Indeed, it is interesting to note that the JBP model crosses the $w = -1$ boundary twice, at $z \gtrsim 0.5$ as well as in the redshift range $2.0 \lesssim z \lesssim 3.0$.

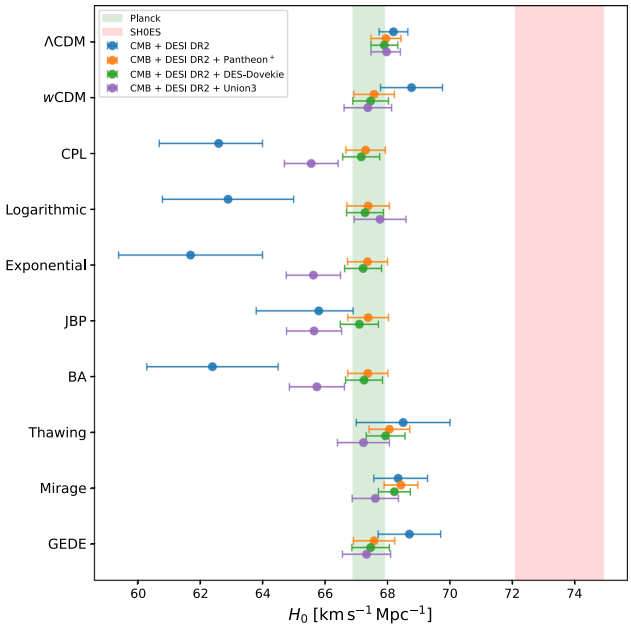

Fig. 4 The figure shows the comparison of the inferred value of the h for ΛCDM, wCDM, Logarithmic, Exponential, CPL, BA, JBP, Thawing, Mirage, and GEDE models. The green vertical band represents the Planck value $H_0 = 67.4 \pm 0.5$ km s^{-1} Mpc^{-1}, while the red vertical band represents the SH0ES measurement $H_0 = 73.5 \pm 1.4$ km s^{-1} Mpc^{-1}

While in the case of the Thawing model this crossing occurs in the redshift range $1.5 \lesssim z \lesssim 2.0$. Finally, in the GEDE model, for the DESI DR2 + CMB dataset combination, the model predicts values in the phantom regime during the entire redshift evolution. In contrast, for the DESI DR2 + CMB + Pantheon$^+$, DESI DR2 + CMB + DES-Dovekie, and DESI DR2 + CMB + Union3 datasets, the predicted values remain above $w = -1$ throughout the full evolution, indicating that there is no phantom crossing in the GEDE model for these dataset combinations.

We find that the combination of DESI DR2 with different SNe Ia samples and compressed CMB likelihoods exhibits a quintom-like evolution of dark energy. In this context, it is important to revisit the *No-Go theorem* associated

Table 4 This table presents the numerical values obtained for the ΛCDM, wCDM, Logarithmic, Exponential, CPL, BA, JBP, Thawing, Mirage, and GEDE models at the 68% (1σ) confidence level, using DESI DR2 measurements combined with different SNe Ia compilations (Pantheon$^+$, DES-Dovekie, Union3) and CMB compressed likelihood

Dataset/Models	H_0	Ω_{m0}	w or w_0	w_a	Δ	$\ln \mathcal{Z}$	$\ln \mathcal{B}_{\text{DE Model},\Lambda\text{CDM}}$	$\Delta\chi^2_{\text{MAP}}$	$N\sigma$
ΛCDM									
CMB + DESI DR2	68.19±0.46	0.3035±0.0056	–	-	–	−20.01	0	0	0
CMB + DESI DR2 + Pantheon$^+$	67.95±0.48	0.3064±0.0058	–	–	–	−723.11	0	0	0
CMB + DESI DR2 + DES-Dovekie	67.90±0.43	0.3072±0.0052	–	–	–	−837.86	0	0	0
CMB + DESI DR2 + Union3	$67.97^{+0.44}_{-0.50}$	0.3064±0.0057	–	–	–	−33.84	0	0	0
wCDM									
CMB + DESI DR2	68.77±0.99	0.2990±0.0085	−1.037±0.041	–	–	−23.33	−3.32	0.29	0
CMB + DESI DR2 + Pantheon$^+$	67.57±0.65	0.3085±0.0065	−0.986±0.026	–	–	−726.58	−3.47	0.22	0
CMB + DESI DR2 + DES-Dovekie	67.46±0.57	0.3094±0.0058	−0.983±0.024	–	–	−841.51	−3.65	−0.02	0.14
CMB + DESI DR2 + Union3	67.37±0.76	0.3103±0.0072	−0.979±0.031	–	–	−37.40	−3.56	0.11	0
CPL									
CMB + DESI DR2	$62.6^{+1.4}_{-1.9}$	$0.366^{+0.023}_{-0.018}$	$-0.33^{+0.23}_{-0.14}$	$-2.07^{+0.34}_{-0.80}$	–	−18.62	1.39	−4.62	1.65
CMB + DESI DR2 + Pantheon$^+$	67.30±0.63	0.3137±0.0067	−0.858±0.058	−0.58±0.24	–	−725.19	−2.08	−2.71	1.13
CMB + DESI DR2 + DES-Dovekie	67.16±0.59	0.3156±0.0065	−0.821±0.059	$-0.73^{+0.27}_{-0.24}$	–	−838.75	−0.89	−4.21	1.55
CMB + DESI DR2 + Union3	65.56±0.86	0.3320±0.0096	−0.662±0.091	−1.15±0.33	–	−32.03	1.81	−6.46	2.06
Logarithmic									
CMB + DESI DR2	62.9±2.1	$0.365^{+0.024}_{-0.028}$	$-0.42^{+0.21}_{-0.25}$	$-1.39^{+0.61}_{-0.47}$	–	−19.42	0.59	−4.40	1.59
CMB + DESI DR2 + Pantheon$^+$	67.38±0.68	0.3138±0.0072	−0.871±0.051	$-0.39^{+0.17}_{-0.16}$	–	−724.77	−1.66	−3.41	1.34
CMB + DESI DR2 + DES-Dovekie	67.28±0.59	0.3151±0.0064	−0.849±0.050	−0.46±0.17	–	−838.76	−0.90	−4.63	1.65
CMB + DESI DR2 + Union3	67.76±0.83	$0.3308^{+0.0084}_{-0.0099}$	−0.710±0.078	$-0.75^{+0.24}_{-0.21}$	–	−32.25	1.59	−6.76	2.12
Exponential									
CMB + DESI DR2	61.7±2.3	$0.379^{+0.028}_{-0.031}$	−0.72±0.11	$-1.06^{+0.41}_{-0.36}$	–	−19.84	0.17	−4.57	1.64
CMB + DESI DR2 + Pantheon$^+$	67.36±0.64	0.3133±0.0068	−0.971±0.027	$-0.230^{+0.11}_{-0.098}$	–	−726.23	−3.12	−2.91	1.19
CMB + DESI DR2 + DES-Dovekie	67.22±0.59	0.3151±0.0065	−0.965±0.025	−0.29±0.11	–	−839.22	−1.36	−4.38	1.59
CMB + DESI DR2 + Union3	65.63±0.87	0.3314±0.0097	−0.898±0.038	−0.48±0.14	–	−32.77	1.07	−6.56	2.08
JBP									
CMB + DESI DR2	$65.8^{+1.1}_{-2.0}$	$0.328^{+0.020}_{-0.012}$	$-0.627^{+0.23}_{-0.086}$	< -1.68	–	−21.88	−1.87	−2.62	1.10
CMB + DESI DR2 + Pantheon$^+$	67.38±0.65	0.3120±0.0066	−0.847±0.080	−0.85±0.49	–	−725.83	−2.72	−1.79	0.83
CMB + DESI DR2 + DES-Dovekie	67.10±0.61	0.3151±0.0065	−0.774±0.085	−1.29±0.52	–	−839.12	−1.26	−3.57	1.38
CMB + DESI DR2 + Union3	65.65±0.88	0.3292±0.0093	$-0.599^{+0.12}_{-0.088}$	$-2.06^{+0.39}_{-0.73}$	–	−33.09	0.75	−5.36	1.82
BA									
CMB + DESI DR2	62.4±2.1	$0.370^{+0.023}_{-0.028}$	$-0.39^{+0.20}_{-0.23}$	$-1.01^{+0.39}_{-0.32}$	–	−19.43	0.58	−4.65	1.66

Table 4 continued

Dataset/Models	H_0	Ω_{m0}	w or w_0	w_a	Δ	$\ln \mathcal{Z}$	$\ln \mathcal{B}_{\text{DE Model, }\Lambda\text{CDM}}$	$\Delta\chi^2_{\text{MAP}}$	$N\sigma$
CMB + DESI DR2 + Pantheon$^+$	67.37±0.64	0.3134±0.0067	−0.881±0.048	−0.26±0.11	–	−725.39	−2.28	−3.17	1.27
CMB + DESI DR2 + DES-Dovekie	67.25±0.59	0.3149±0.0063	−0.856±0.048	−0.31±0.12	–	−838.94	−1.08	−4.37	1.59
CMB + DESI DR2 + Union3	65.74±0.88	0.3306±0.0097	−0.722±0.078	−0.51±0.15	–	−32.44	−1.40	−6.61	2.09
Thawing									
CMB + DESI DR2	68.5±1.5	0.304±0.013	−0.956±0.090	–	–	−20.01	0.00	−2.71	1.65
CMB + DESI DR2 + Pantheon$^+$	68.06±0.65	0.3077±0.0064	−0.930±0.040	–	–	−722.24	0.87	−3.83	1.96
CMB + DESI DR2 + DES-Dovekie	67.94±0.62	0.3087±0.0064	−0.921±0.037	–	–	−836.68	1.18	−4.42	2.10
CMB + DESI DR2 + Union3	67.23±0.83	0.3151±0.0081	−0.887±0.052	–	–	−32.30	1.54	−4.94	2.22
Mirage									
CMB + DESI DR2	$68.34^{+0.94}_{-0.78}$	$0.3079^{+0.0091}_{-0.011}$	$-0.87^{+0.10}_{-0.13}$	–	–	−19.25	0.76	−2.98	1.73
CMB + DESI DR2 + Pantheon$^+$	68.43±0.54	0.3071±0.0065	−0.889±0.058	–	–	−721.56	1.55	−3.93	1.98
CMB + DESI DR2 + DES-Dovekie	68.22±0.51	0.3095±0.0061	−0.856±0.059	–	–	−835.67	2.19	−5.00	2.24
CMB + DESI DR2 + Union3	67.61±0.74	0.3166±0.0088	−0.767±0.095	–	–	−30.89	2.95	−5.37	2.32
GEDE									
CMB + DESI DR2	68.8±1.0	0.2994±0.0087	–	–	$0.13^{+0.26}_{-0.30}$	−21.78	−1.77	−0.64	0.80
CMB + DESI DR2 + Pantheon$^+$	67.69±0.63	0.3084±0.0061	–	–	−0.17±0.17	−724.38	−1.27	−0.95	0.97
CMB + DESI DR2 + DES-Dovekie	67.58±0.58	0.3093±0.0059	–	–	−0.20±0.16	−839.33	−1.47	−1.24	1.11
CMB + DESI DR2 + Union3	67.43±0.81	0.3105±0.0077	–	–	−0.24±0.22	−35.39	−1.55	−1.15	1.07

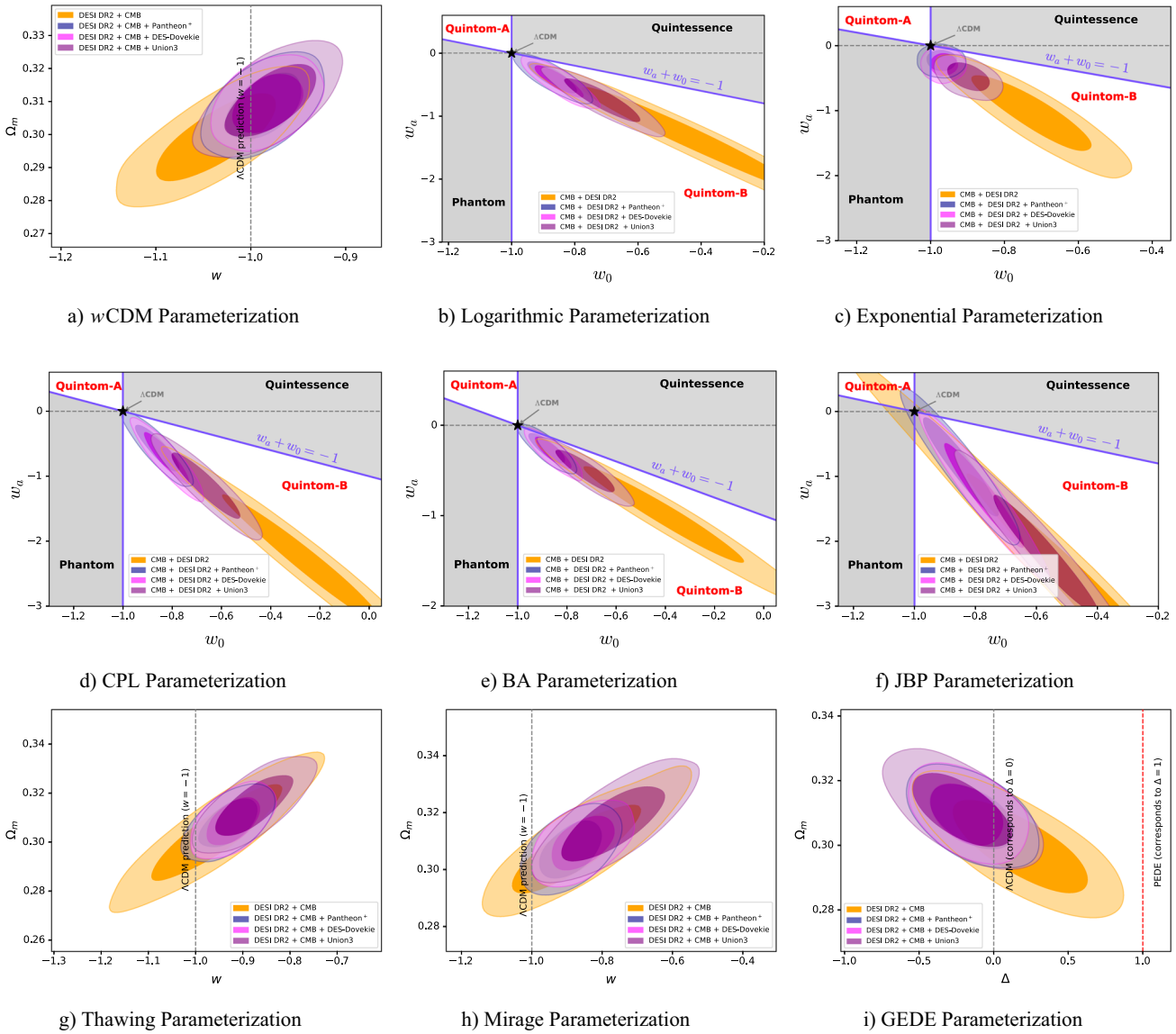

a) wCDM Parameterization b) Logarithmic Parameterization c) Exponential Parameterization

d) CPL Parameterization e) BA Parameterization f) JBP Parameterization

g) Thawing Parameterization h) Mirage Parameterization i) GEDE Parameterization

Fig. 5 The figure shows the posterior distributions of different planes of the wCDM, Logarithmic, Exponential, CPL, BA, JBP, Thawing, Mirage, and GEDE models using DESI DR2 measurements combined with different SNe Ia compilations (Pantheon$^+$, DES-Dovekie, Union3) and CMB compressed likelihood, at the 68% (1σ) and 95% (2σ) confidence intervals

with dynamical dark energy [158,159]. In particular, a single canonical scalar field or a single perfect fluid model cannot reproduce such quintom-like behavior, as these frameworks forbid the equation-of-state parameter w from crossing the cosmological constant boundary $w = -1$ [160,161].

It is important to emphasize that such behavior can also be partly induced by the choice of the EoS parametrization, and should therefore be interpreted with caution. In particular, parameters such as (w_0, w_a) correspond to an effective parametrization fitted over a limited redshift range, and extrapolating this parametrization over the full cosmic history can be misleading. While it is often stated that quintessence models lie above the line $w_0 + w_a = -1$, this is not strictly correct. Although the true equation of state $w(a)$ for canonical quintessence cannot cross the phantom divide $w = -1$, the fitted parametrization may still occupy regions in the (w_0, w_a) plane that formally imply a phantom crossing when extrapolated beyond the fitted redshift range.

Recent studies have demonstrated that quintessence models can populate more negative regions of the (w_0, w_a) plane when the parametrization is fitted to the model [162–164], and have also highlighted subtleties in the interpretation of such parametrizations [165]. Therefore, an apparent phantom crossing inferred from (w_0, w_a) should not be directly interpreted as evidence for true phantom dynamics, but rather as

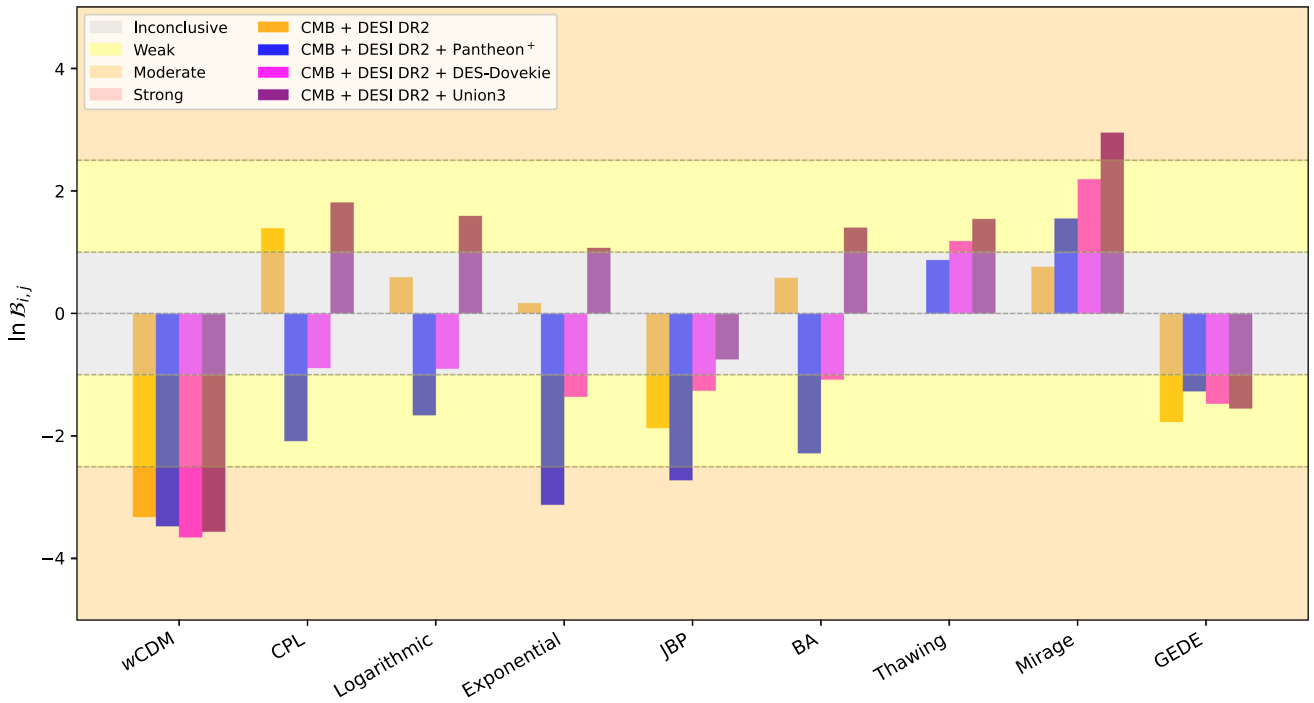

Fig. 6 The figure shows the relative difference ($\ln \mathcal{B}_{i,j}$) of the Bayes factor in logarithmic space compared to the ΛCDM model, using DESI DR2 measurements combined with different SNe Ia compilations (Pantheon$^+$, DES-Dovekie, Union3) and the CMB compressed likelihood

a feature of the effective parametrization within the redshift range probed by the data.

Figure 8 shows the redshift evolution of the energy density function for the CPL, Logarithmic, Exponential, JBP, BA, and Mirage models. For all dataset combinations, $f_{DE}(z)$ crosses $f_{DE} = 1$ and converges to unity at the present epoch, $z = 0$, i.e., $f_{DE}(0) = 1$. In contrast, for the Thawing and GEDE models, $f_{DE}(z)$ remains above unity ($f_{DE} > 1$) throughout the evolution and only approaches $f_{DE}(0) = 1$ at $z = 0$. In both figures, the solid lines represent the mean values, while the light and dark shaded regions correspond to the 1σ and 2σ confidence intervals, respectively.

5 Conclusions

This study provides evidence suggestive of the evolving nature of dark energy, though not yet conclusive, challenging the core assumptions of the standard ΛCDM model with a cosmological constant. In particular, our analysis of DESI DR2 indicates that the LRG1 and LRG3+ELG1 tracers introduce tensions in the inferred value of Ω_m, highlighting their key role in driving deviations from ΛCDM.

Extending the analysis beyond ΛCDM, we find that the inclusion of LRG1-2 tracers systematically shifts the inferred parameters of dynamical dark energy models, particularly toward $w_0 > -1$. When combined with CMB and SNe Ia datasets, the constraints in the w_0-w_a plane tend to occupy the region ($w_0 > -1$, $w_a < 0$), suggesting a quintom-like evolution at a phenomenological level.

Using the $\Delta\chi^2_{\rm MAP}$ statistic, we find that the preference for dynamical dark energy remains at the weak-to-moderate level, typically corresponding to $N\sigma \sim$ 1-2.3, depending on the model and dataset combination, with the largest values generally obtained for the Union3 dataset. Thus, no dynamical dark energy model is consistently preferred over ΛCDM, and current data provide only mild, non-decisive hints of evolution.

The reconstructed evolution of the equation-of-state parameter $w(z)$ exhibits indications of phantom crossing behavior in several parametrizations. However, according to the theoretical no-go theorem, such behavior cannot arise in single canonical scalar-field or perfect fluid models, and should therefore be interpreted with caution. In addition, part of this behavior may be induced by the choice of parametrization, rather than reflecting a fundamental physical effect.

The Bayesian analysis further supports this interpretation, showing that ΛCDM remains statistically competitive across all dataset combinations, with no model demonstrating a robust or consistent preference over it. These results indicate that, while phenomenological features of evolving dark energy appear in certain cases, they do not yet provide decisive evidence for a departure from the concordance cosmological model.

These findings highlight that our current understanding of DE may be incomplete, although present data do not

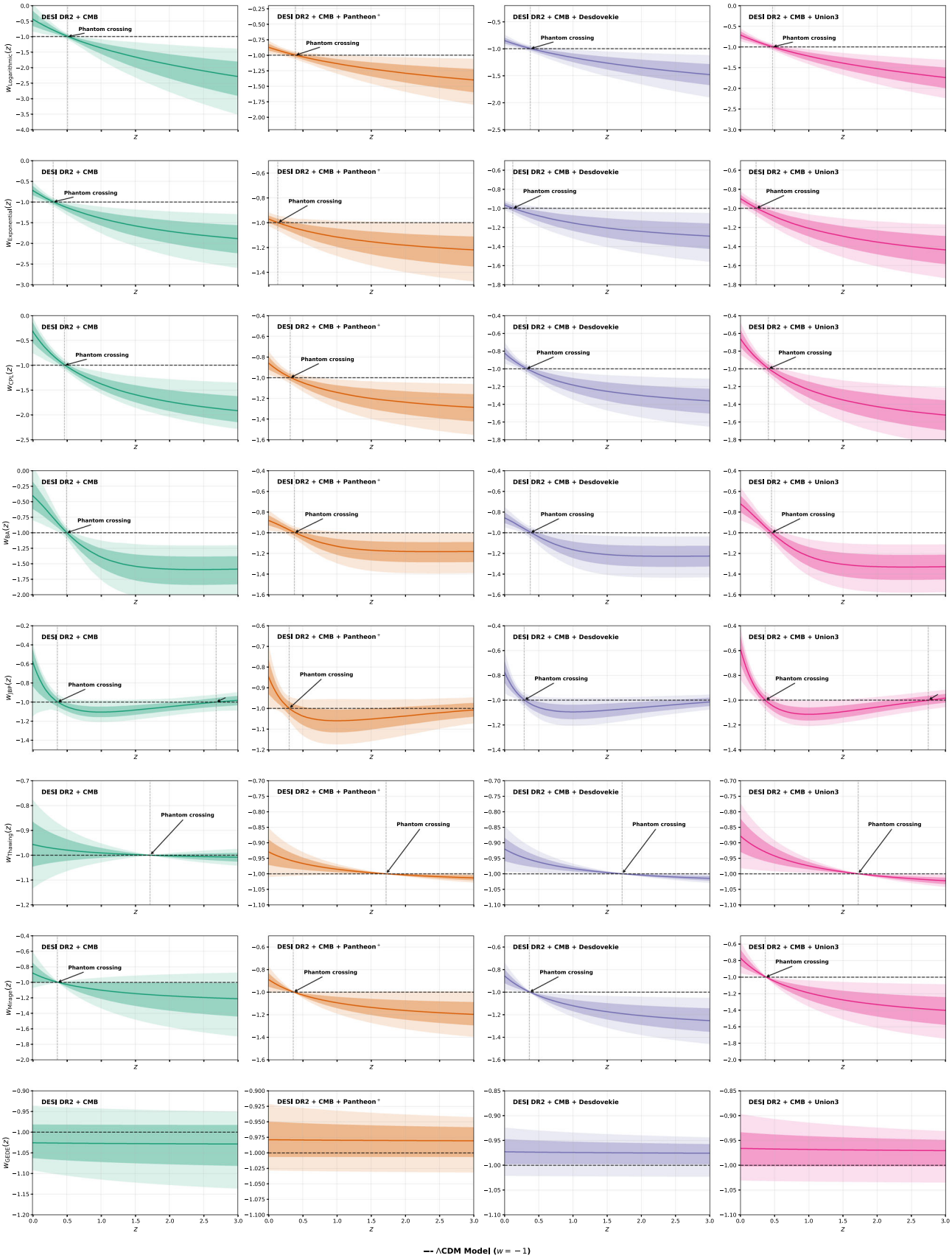

Fig. 7 This figure shows the evolution of $w(z)$ as a function of redshift, using DESI DR2 measurements combined with different SNe Ia compilations (Pantheon$^+$, DES-Dovekie, Union3) and CMB compressed likelihood

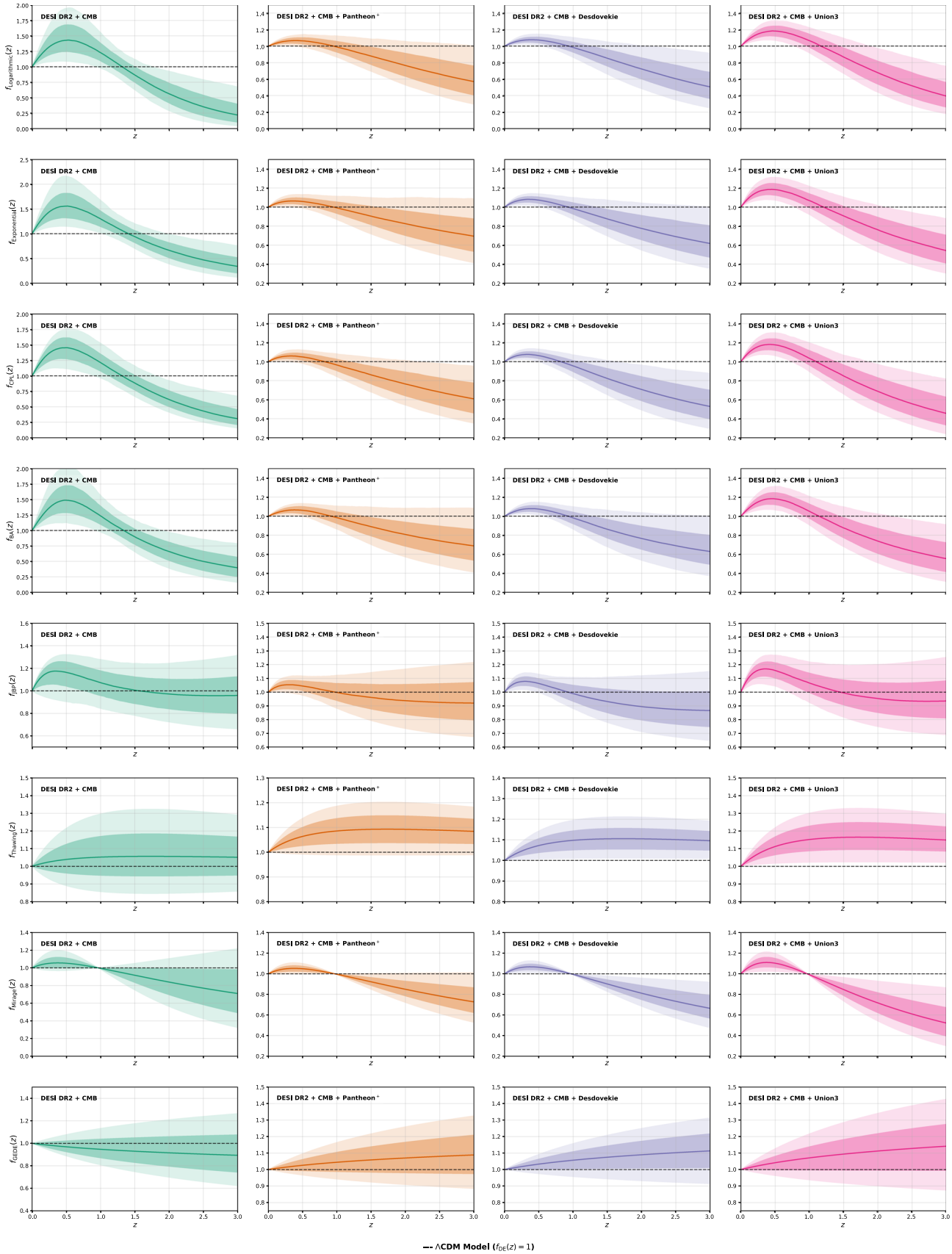

Fig. 8 This figure shows the evolution of $f_{DE}(z)$ as a function of redshift, using DESI DR2 measurements combined with different SNe Ia compilations (Pantheon^{+}, DES-Dovekie, Union3) and CMB compressed likelihood

yet require a departure from the ΛCDM framework. If confirmed, the evolving nature of DE could significantly impact our understanding of the Universe expansion and may require a reevaluation of the fundamental assumptions underlying cosmology. Therefore, further investigation and more precise measurements, particularly at low redshifts, are essential to fully characterize the nature of DE and its role in shaping the cosmos

Acknowledgements SC acknowledges the Istituto Nazionale di Fisica Nucleare (INFN) Sez. di Napoli, Iniziative Specifiche QGSKY and MoonLight-2 and the Istituto Nazionale di Alta Matematica (INdAM), gruppo GNFM, for the support. This paper is based upon work from COST Action CA21136 – Addressing observational tensions in cosmology with systematics and fundamental physics (CosmoVerse), supported by COST (European Cooperation in Science and Technology).

Data Availability Statement Data will be made available on reasonable request. [Authors' comment: The BAO data from DESI DR2, which are available at [CobayaSampler bao_data](https://github.com/CobayaSampler/bao_data.). The Pantheon+ data are available at [PantheonPlusSH0ES DataRelease](https://github.com/PantheonPlusSH0ES/DataRelease.git), the DES-Dovekie data are available at [DES-SN5YR](https://github.com/des-science/DES-SN5YR.git), and the Union3 data are available at [union3_release](https://github.com/rubind/union3_release.git)].

Code Availability Statement Code/software will be made available on reasonable request. [Authors' comment: The SimpleMC code, which is available here [SimpleMC](https://github.com/ja-vazquez/SimpleMC.git)].

Funded by SCOAP[3].

References

1. A.G. Riess et al., Observational evidence from supernovae for an accelerating universe and a cosmological constant. Astron. J. **116**, 1009–1038 (1998)
2. S. Perlmutter et al., Measurements of Ω and Λ from 42 high redshift supernovae. Astrophys. J. **517**, 565–586 (1999)
3. K. Bamba, S. Capozziello, S. Nojiri, S.D. Odintsov, Dark energy cosmology: the equivalent description via different theoretical models and cosmography tests. Astrophys. Space Sci. **342**, 155–228 (2012)
4. A. Sousa-Neto, C. Bengaly, J.E. Gonzalez, J. Alcaniz, Symbolic regression analysis of dynamical dark energy with DESI-DR2 and SN data. Phys. Dark Univ. **50**, 102108 (2025)
5. A. Adame, J. Aguilar, S. Ahlen, S. Alam, D. Alexander, M. Alvarez, O. Alves, A. Anand, U. Andrade, E. Armengaud et al., Desi 2024 vi: cosmological constraints from the measurements of baryon acoustic oscillations. J. Cosmol. Astropart. Phys. **2025**(02), 021 (2025)
6. R. Calderon et al., DESI 2024: reconstructing dark energy using crossing statistics with DESI DR1 BAO data. JCAP **10**, 048 (2024)
7. M.A. Karim, J. Aguilar, S. Ahlen, S. Alam, L. Allen, C.A. Prieto, O. Alves, A. Anand, U. Andrade, E. Armengaud, Desi dr2 results. ii. measurements of baryon acoustic oscillations and cosmological constraints. Phys. Rev. D 112(8), (2025)
8. K. Lodha, A. Shafieloo, R. Calderon, E. Linder, W. Sohn, J. Cervantes-Cota, A. De Mattia, J. García-Bellido, M. Ishak, W. Matthewson et al., Desi 2024: Constraints on physics-focused aspects of dark energy using desi dr1 bao data. Phys. Rev. D **111**(2), 023532 (2025)
9. K. Lodha et al., Extended dark energy analysis using DESI DR2 BAO measurements. Phys. Rev. D **112**(8), 083511 (2025)
10. A. Notari, M. Redi, A. Tesi, BAO vs. SN evidence for evolving dark energy. JCAP **04**, 048 (2025)
11. I. Dymnikova, M.Y. Khlopov, Self-consistent initial conditions in inflationary cosmology. Gravitation Cosmol. **4**, 50–55 (1998)
12. I. Dymnikova, M. Khlopov, Decay of cosmological constant as bose condensate evaporation. Mod. Phys. Lett. A **15**(38n39), 2305–2314 (2000)
13. I. Dymnikova, M. Khlopov, Decay of cosmological constant in self-consistent inflation. Euro. Phys. J. C-Particles Fields **20**(1), 139–146 (2001)
14. S. Ray, M. Khlopov, P.P. Ghosh, U. Mukhopadhyay, Phenomenology of λ-cdm model: a possibility of accelerating universe with positive pressure. Int. J. Theor. Phys. **50**(3), 939–951 (2011)
15. A. Doroshkevich, M.Y. Khlopov, Formation of structure in a universe with unstable neutrinos. Mon. Not. R. Astron. Soc. **211**(2), 277–282 (1984)
16. P. A. Ade, N. Aghanim, C. Armitage-Caplan, M. Arnaud, M. Ashdown, F. Atrio-Barandela, J. Aumont, C. Baccigalupi, A. J. Banday, R. Barreiro, et al., Planck 2013 results. xvi. cosmological parameters, Astron. Astrophys.U 571, A16 (2014)
17. M. Betoule, R. Kessler, J. Guy, J. Mosher, D. Hardin, R. Biswas, P. Astier, P. El-Hage, M. Konig, S. Kuhlmann et al., Improved cosmological constraints from a joint analysis of the sdss-ii and snls supernova samples. Astron. Astrophys. **568**, A22 (2014)
18. P.A. Ade, N. Aghanim, M. Arnaud, M. Ashdown, J. Aumont, C. Baccigalupi, A. Banday, R. Barreiro, J. Bartlett, N. Bartolo et al., Planck 2015 results-xiii. cosmological parameters. Astron. Astrophys. **594**, A13 (2016)
19. D. Brout, D. Scolnic, B. Popovic, A.G. Riess, A. Carr, J. Zuntz, R. Kessler, T.M. Davis, S. Hinton, D. Jones et al., The pantheon+ analysis: cosmological constraints. Astrophys. J. **938**(2), 110 (2022)
20. D. Rubin, G. Aldering, M. Betoule, A. Fruchter, X. Huang, A.G. Kim, C. Lidman, E. Linder, S. Perlmutter, P. Ruiz-Lapuente et al., Union through unity: Cosmology with 2000 sne using a unified bayesian framework. Astrophys. J. **986**(2), 231 (2025)
21. B. Popovic, P. Shah, W. Kenworthy, R. Kessler, T. Davis, A. Goobar, D. Scolnic, M. Vincenzi, P. Wiseman, R. Chen, The dark energy survey supernova program: A reanalysis of cosmology results and evidence for evolving dark energy with an updated type ia supernova calibration (2025). arXiv:2511.07517
22. L. Huang, R.-G. Cai, S.-J. Wang, The DESI DR1/DR2 evidence for dynamical dark energy is biased by low-redshift supernovae. Sci. China Phys. Mech. Astron. **68**(10), 100413 (2025)
23. I.D. Gialamas, G. Hütsi, K. Kannike, A. Racioppi, M. Raidal, M. Vasar, H. Veermäe, Interpreting desi 2024 bao: late-time dynamical dark energy or a local effect? Phys. Rev. D **111**(4), 043540 (2025)
24. G. Efstathiou, Evolving dark energy or supernovae systematics? Mon. Not. R. Astron. Soc. **538**(2), 875–882 (2025)

25. M. Cortês, A. R. Liddle, On desi's dr2 exclusion of λcdm, Monthly Notices of the Royal Astronomical Society: Letters. slaf108 (2025)
26. M. Scherer, M.A. Sabogal, R.C. Nunes, A. De Felice, Challenging the ΛCDM model: 5σ evidence for a dynamical dark energy late-time transition. Phys. Rev. D **112**(4), 043513 (2025)
27. S. Barua, S. Desai, Constraints on dark energy models using late Universe probes. Phys. Dark Univ. **49**, 101995 (2025)
28. S. Vilardi, S. Capozziello, M. Brescia, Discriminating between cosmological models using data-driven methods. Astron. Astrophys. **695**, A166 (2025)
29. W. Yin, Cosmic clues: Desi, dark energy, and the cosmological constant problem. J. High Energy Phys. **2024**(5), 1–9 (2024)
30. M. Cortês, A.R. Liddle, Interpreting desi's evidence for evolving dark energy. J. Cosmol. Astropart. Phys. **2024**(12), 007 (2024)
31. Y. Carloni, O. Luongo, M. Muccino, Does dark energy really revive using desi 2024 data? Phys. Rev. D **111**(2), 023512 (2025)
32. N. Roy, Dynamical dark energy in the light of desi 2024 data. Phys. Dark Univ. **48**, 101912 (2025)
33. L. Orchard, V.H. Cárdenas, Probing dark energy evolution post-desi 2024. Phys. Dark Univ. **46**, 101678 (2024)
34. W. Giarè, M. Najafi, S. Pan, E. Di Valentino, J.T. Firouzjaee, Robust preference for dynamical dark energy in desi bao and sn measurements. J. Cosmol. Astropart. Phys. **2024**(10), 035 (2024)
35. Y.-H. Pang, X. Zhang, Q.-G. Huang, Constraints on redshift-binned dark energy using desi bao data. Phys. Rev. D **111**(12), 123504 (2025)
36. W.J. Wolf, C. García-García, P.G. Ferreira, Robustness of dark energy phenomenology across different parameterizations. J. Cosmol. Astropart. Phys. **2025**(05), 034 (2025)
37. Q. Gao, Z. Peng, S. Gao, Y. Gong, On the evidence of dynamical dark energy. Universe **11**(1), 10 (2024)
38. W. Giarè, T. Mahassen, E.D. Valentino, S. Pan, An overview of what current data can (and cannot yet) say about evolving dark energy. Phys. Dark Univ. 101906 (2025)
39. E.Ó. Colgáin, S. Pourojaghi, M.M. Sheikh-Jabbari, L. Yin, How much has DESI dark energy evolved since DR1? Phys. Dark Univ. **52**, 102268 (2026)
40. C.-G. Park, J. de Cruz Pérez, B. Ratra, Is the w_0w_aCDM cosmological parameterization evidence for dark energy dynamics partially caused by the excess smoothing of Planck CMB anisotropy data?, Int. J. Mod. Phys. D 34 (13) 2550058 (2025)
41. E. Fazzari, W. Giarè, E. Di Valentino, Cosmographic footprints of dynamical dark energy. Astrophys. J. Lett. **996**(1), L5 (2026)
42. J. Moffat, E. Thompson, Dynamical dark energy at late time λcdm, arXiv:2505.18900 (2025)
43. S.H. Mirpoorian, K. Jedamzik, L. Pogosian, Is dynamical dark energy necessary? DESI BAO and modified recombination. JCAP **12**, 050 (2025)
44. M. W. Toomey, G. Montefalcone, E. McDonough, K. Freese, How theory-informed priors affect desi evidence for evolving dark energy, arXiv:2509.13318 (2025)
45. M. Ishak, L. Medina-Varela, Persistent and serious challenge to the λcdm throne: Evidence for dynamical dark energy rising from combinations of different types of datasets, arXiv:2507.22856 (2025)
46. D.-C. Qiang, J.-Y. Jia, H. Wei, New insights into dark energy from desi dr2 with cmb and snia (2025). arXiv:2507.09981
47. S. Capozziello, H. Chaudhary, T. Harko, G. Mustafa, Is dark energy dynamical in the desi era? a critical review. Phys. Dark Univ. 102196 (2025)
48. V.K. Sharma, H. Chaudhary, S. Kolekar, Probing generalized emergent dark energy with desi dr2. J. High Energy Astrophys. 100518 (2025)
49. H. Chaudhary, S. Capozziello, S. Praharaj, S. K. J. Pacif, G. Mustafa, Is the λcdm model in crisis?, J. High Energy Astrophys. 100507 (2025)
50. S. Capozziello, H. Chaudhary, G. Mustafa, S. Pacif, Evidence for dynamical dark energy using desi dr2 lyα forest, arXiv:2510.21976 (2025)
51. H. Chaudhary, S. Capozziello, V.K. Sharma, G. Mustafa, Does desi dr2 challenge λcdm paradigm? Astrophys. J. **992**(2), 194 (2025)
52. H. Chaudhary, V.K. Sharma, S. Capozziello, G. Mustafa, Probing departures from ΛCDM by late-time datasets. Astrophys. J. Suppl. **283**(2), 73 (2026)
53. P. Mukherjee, A.A. Sen, Model-independent cosmological inference post desi dr1 bao measurements. Phys. Rev. D **110**(12), 123502 (2024)
54. B.R. Dinda, R. Maartens, Model-agnostic assessment of dark energy after desi dr1 bao. J. Cosmol. Astropart. Phys. **2025**(01), 120 (2025)
55. J.-Q. Jiang, D. Pedrotti, S.S. da Costa, S. Vagnozzi, Nonparametric late-time expansion history reconstruction and implications for the hubble tension in light of recent desi and type ia supernovae data. Phys. Rev. D **110**(12), 123519 (2024)
56. M. Tsedrik, S. Lee, K. Markovic, P. Carrilho, A. Pourtsidou, C. Moretti, B. Bose, E. Huff, A. Robertson, P. Taylor et al., Interacting dark energy constraints from the full-shape analyses of boss dr12 and des year 3 measurements. Mon. Notices R. Astron. Soc. **541**(1), L65–L70 (2025)
57. J.-X. Li, S. Wang, Reconstructing dark energy with model independent methods after DESI DR2. Eur. Phys. J. C **85**(11), 1308 (2025)
58. Y. Wang, K. Freese, Model-independent dark energy measurements from DESI DR2 and Planck 2015 data. JCAP **02**, 023 (2026)
59. P.-J. Wu, T.-N. Li, G.-H. Du, X. Zhang, Observational challenges to holographic and ricci dark energy paradigms: Insights from act dr6 and desi dr2. Chin. Phys. C **50**(4), 045105 (2026)
60. F. Plaza, G. León, L. Kraiselburd, Probing the h 0 tension with holographic dark energy in unimodular gravity: insights from desi dr2. Euro. Phys. J. C **85**(11), 1262 (2025)
61. T.-N. Li, P.-J. Wu, G.-H. Du, Y.-H. Yao, J.-F. Zhang, X. Zhang, Exploring non-cold dark matter in the scenario of dynamical dark energy with desi dr2 data, Physics of the Dark Universe. 102068 (2025)
62. M. Braglia, X. Chen, A. Loeb, Exotic dark matter and the DESI anomaly. JCAP **11**, 064 (2025)
63. S.S. Mishra, W.L. Matthewson, V. Sahni, A. Shafieloo, Y. Shtanov, Braneworld dark energy in light of DESI DR2. JCAP **11**, 018 (2025)
64. S. Goldstein, M. Celoria, F. Schmidt, Monodromic dark energy and desi. Phys. Rev. D **113**(2), 023532 (2026)
65. Y. Tada, T. Terada, Quintessential interpretation of the evolving dark energy in light of desi observations. Phys. Rev. D **109**(12), L121305 (2024)
66. S. Bhattacharya, G. Borghetto, A. Malhotra, S. Parameswaran, G. Tasinato, I. Zavala, Cosmological constraints on curved quintessence. J. Cosmol. Astropart. Phys. **2024**(09), 073 (2024)
67. O.F. Ramadan, J. Sakstein, D. Rubin, Desi constraints on exponential quintessence. Phys. Rev. D **110**(4), L041303 (2024)
68. I.D. Gialamas, G. Hütsi, M. Raidal, J. Urrutia, M. Vasar, H. Veermäe, Quintessence and phantoms in light of desi 2025. Phys. Rev. D **112**(6), 063551 (2025)
69. B.R. Dinda, R. Maartens, Physical versus phantom dark energy after desi: thawing quintessence in a curved background. Mon. Notices R. Astron. Soc. **542**(1), L31–L35 (2025)

70. H. Adam, M.P. Hertzberg, D. Jiménez-Aguilar, I. Khan, Comparing minimal and non-minimal quintessence models to 2025 desi data. arXiv:2509.13302 (2025)
71. V. Petri, V. Marra, R. von Marttens, Dark degeneracy in DESI DR2 data: Interacting or evolving dark energy? Phys. Rev. D **113**(2), 023504 (2026)
72. J.-Q. Wang, R.-G. Cai, Z.-K. Guo, S.-J. Wang, Resolving the planck-desi tension by non-minimally coupled quintessence, arXiv preprint arXiv:2508.01759 (2025)
73. K.V. Berghaus, J.A. Kable, V. Miranda, Quantifying scalar field dynamics with desi 2024 y1 bao measurements. Phys. Rev. D **110**(10), 103524 (2024)
74. R. Mazumdar, M.M. Gohain, K. Bhuyan, Constraint on symmetric teleparallel gravity with different dark energy parametrizations from desi dr2 bao data. arXiv:2507.05975 (2025)
75. T. Liu, X. Li, T. Xu, M. Biesiada, J. Wang, Torsion cosmology in the light of DESI, supernovae and CMB observational constraints. Eur. Phys. J. C **85**(11), 1351 (2025)
76. G. Ye, S.-J. Lin, On the tension between desi dr2 bao and cmb. arXiv:2505.02207 (2025)
77. H. An, C. Han, B. Zhang, Topological defects as effective dynamical dark energy. Phys. Rev. D **113**(4), 043543 (2026)
78. S.R. Choudhury, T. Okumura, Updated cosmological constraints in extended parameter space with planck pr4, desi baryon acoustic oscillations, and supernovae: Dynamical dark energy, neutrino masses, lensing anomaly, and the hubble tension. Astrophys. J. Lett. **976**(1), L11 (2024)
79. S. Roy Choudhury, Cosmology in Extended Parameter Space with DESI Data Release 2 Baryon Acoustic Oscillations: A $2\sigma+$ Detection of Nonzero Neutrino Masses with an Update on Dynamical Dark Energy and Lensing Anomaly, Astrophys. J. Lett. 986 (2), L31 (2025)
80. J. Rebouças, D.H. de Souza, K. Zhong, V. Miranda, R. Rosenfeld, Investigating late-time dark energy and massive neutrinos in light of desi y1 bao. J. Cosmol. Astropart. Phys. **2025**(02), 024 (2025)
81. E. Silva, M.A. Sabogal, M. Scherer, R.C. Nunes, E. Di Valentino, S. Kumar, New constraints on interacting dark energy from desi dr2 bao observations. Phys. Rev. D **111**(12), 123511 (2025)
82. H. Wang, Y.-S. Piao, Dark energy in light of DESI DR1 and Hubble tension. Phys. Lett. B **873**, 140180 (2026)
83. S. Vagnozzi, New physics in light of the h_0 tension: an alternative view. Phys. Rev. D **102**(2), 023518 (2020)
84. S. Vagnozzi, Seven hints that early-time new physics alone is not sufficient to solve the hubble tension. Universe **9**(9), 393 (2023)
85. D. Pedrotti, L.A. Escamilla, V. Marra, L. Perivolaropoulos, S. Vagnozzi, BAO miscalibration cannot rescue late-time solutions to the Hubble tension. Phys. Rev. D **113**(4), 043507 (2026)
86. M. Benetti, S. Capozziello, Connecting early and late epochs by $f(z)$CDM cosmography. JCAP **12**, 008 (2019)
87. A.T. Petreca, M. Benetti, S. Capozziello, Beyond ΛCDM with $f(z)$CDM: Criticalities and solutions of Padé Cosmography. Phys. Dark Univ. **44**, 101453 (2024)
88. E.V. Linder, The mirage of $w = -1$. arXiv:0708.0024 (2007)
89. G. Efstathiou, Constraining the equation of state of the universe from distant type ia supernovae and cosmic microwave background anisotropies. Mon. Not. R. Astron. Soc. **310**(3), 842–850 (1999)
90. R. Silva, R. Goncalves, J. Alcaniz, H. Silva, Thermodynamics and dark energy. Astron. Astrophys. **537**, A11 (2012)
91. M. Najafi, S. Pan, E. Di Valentino, J.T. Firouzjaee, Dynamical dark energy confronted with multiple cmb missions. Phys. Dark Univ. **45**, 101539 (2024)
92. M. Chevallier, D. Polarski, Accelerating universes with scaling dark matter. International Journal of Modern Physics D **10**(02), 213–223 (2001)
93. E.V. Linder, Exploring the expansion history of the universe. Phys. Rev. Lett. **90**(9), 091301 (2003)
94. E. Barboza Jr., J. Alcaniz, A parametric model for dark energy. Phys. Lett. B **666**(5), 415–419 (2008)
95. H. Jassal, J. Bagla, T. Padmanabhan, Wmap constraints on low redshift evolution of dark energy. Mon. Notices R. Astron. Soc. **356**(1), L11–L16 (2005)
96. X. Li, A. Shafieloo, Evidence for emergent dark energy. Astrophys. J. **902**(1), 58 (2020)
97. F. Feroz, M.P. Hobson, Multimodal nested sampling: an efficient and robust alternative to markov chain monte carlo methods for astronomical data analyses. Mon. Not. R. Astron. Soc. **384**(2), 449–463 (2008)
98. F. Feroz, M.P. Hobson, E. Cameron, A.N. Pettitt, Importance Nested Sampling and the MultiNest Algorithm. Open J. Astrophys. **2**(1), 10 (2019)
99. J.S. Speagle, dynesty: a dynamic nested sampling package for estimating bayesian posteriors and evidences. Mon. Not. R. Astron. Soc. **493**(3), 3132–3158 (2020)
100. R.E. Kass, A.E. Raftery, Bayes factors. J. Am. Stat. Assoc. **90**(430), 773–795 (1995)
101. A. Lewis, Getdist: a python package for analysing monte carlo samples. J. Cosmol. Astropart. Phys. **2025**(08), 025 (2025)
102. N. Aghanim, Y. Akrami, M. Ashdown, J. Aumont, C. Baccigalupi, M. Ballardini, A.J. Banday, R. Barreiro, N. Bartolo, S. Basak et al., Planck 2018 results-vi. cosmological parameters. Astron. Astrophys. **641**, A6 (2020)
103. M. Hicken, P. Challis, S. Jha, R.P. Kirshner, T. Matheson, M. Modjaz, A. Rest, W.M. Wood-Vasey, G. Bakos, E.J. Barton et al., Cfa 3: 185 type ia supernova light curves from the cfa. Astrophys. J. **700**(1), 331 (2009)
104. M. Hicken, P. Challis, R.P. Kirshner, A. Rest, C.E. Cramer, W.M. Wood-Vasey, G. Bakos, P. Berlind, W.R. Brown, N. Caldwell et al., Cfa4: light curves for 94 type ia supernovae. Astrophys. J. Suppl. Ser. **200**(2), 12 (2012)
105. R. Foley, Foundation supernova survey. Keck Obs. Arch. **U079**, 39 (2017)
106. D.C.T. Abbott, M. Acevedo, M. Aguena, A. Alarcon, S. Allam, O. Alves, A. Amon, F. Andrade-Oliveira, J. Annis, P. Armstrong et al., The dark energy survey: cosmology results with 1500 new high-redshift type ia supernovae using the full 5 yr data set. Astrophys. J. Lett **973**(1), L14 (2024)
107. M. Goliath, R. Amanullah, P. Astier, A. Goobar, R. Pain, Supernovae and the nature of the dark energy. Astron. Astrophys. **380**(1), 6–18 (2001)
108. L.A. Escamilla, W. Giarè, E. Di Valentino, R.C. Nunes, S. Vagnozzi, The state of the dark energy equation of state circa 2023. J. Cosmol. Astropart. Phys. **2024**(05), 091 (2024)
109. E. Komatsu, J. Dunkley, M. Nolta, C.L. Bennett, B. Gold, G. Hinshaw, N. Jarosik, D. Larson, M. Limon, L. Page et al., Five-year wilkinson microwave anisotropy probe* observations: cosmological interpretation. Astrophys. J. Suppl. Ser. **180**(2), 330 (2009)
110. E.Ó. Colgáin, M.G. Dainotti, S. Capozziello, S. Pourojaghi, M. Sheikh-Jabbari, D. Stojkovic, Does desi, confirm λcdm? Journal of High Energy Astrophysics **2025**, 100428 (2024)
111. E.Ó. Colgáin, M. Sheikh-Jabbari, R. Solomon, G. Bargiacchi, S. Capozziello, M.G. Dainotti, D. Stojkovic, Revealing intrinsic flat λ cdm biases with standardizable candles. Physical Review D **106**(4), L041301 (2022)
112. J. Zheng, D.-C. Qiang, Z.-Q. You, Cosmological constraints on dark energy models using DESI BAO 2024. JCAP **08**, 056 (2025)
113. E.Ó. Colgáin, M. Sheikh-Jabbari, R. Solomon, M.G. Dainotti, D. Stojkovic, Putting flat λcdm in the (redshift) bin. Phys. Dark Univ. **44**, 101464 (2024)
114. M.G. Dainotti, B. De Simone, T. Schiavone, G. Montani, E. Rinaldi, G. Lambiase, M. Bogdan, S. Ugale, On the evolution of

the hubble constant with the sne ia pantheon sample and baryon acoustic oscillations: a feasibility study for grb-cosmology in 2030. Galaxies **10**(1), 24 (2022)
115. M.G. Dainotti, B. De Simone, T. Schiavone, G. Montani, E. Rinaldi, G. Lambiase, On the hubble constant tension in the sne ia pantheon sample. Astrophys. J. **912**(2), 150 (2021)
116. X. Jia, J. Hu, F. Wang, Evidence of a decreasing trend for the hubble constant. Astronomy & Astrophysics **674**, A45 (2023)
117. E. Pastén, V.H. Cárdenas, Testing λcdm cosmology in a binned universe: Anomalies in the deceleration parameter. Phys. Dark Univ. **40**, 101224 (2023)
118. M. Malekjani, R. Mc Conville, E.Ó. Colgáin, S. Pourojaghi, M. Sheikh-Jabbari, On redshift evolution and negative dark energy density in pantheon+ supernovae. Euro. Phys. J. C. **84**(3), 317 (2024)
119. J. Wagner, Solving the Hubble tension à la Ellis & Stoeger 1987, PoS CORFU2022, 267 (2023)
120. J.-P. Hu, F.-Y. Wang, Revealing the late-time transition of h 0: relieve the hubble crisis. Mon. Not. R. Astron. Soc. **517**(1), 576–581 (2022)
121. M. Dainotti, B. De Simone, G. Montani, T. Schiavone, G. Lambiase, The Hubble constant tension: current status and future perspectives through new cosmological probes, PoS CORFU2022, 235 (2023)
122. C. Krishnan, E.Ó. Colgáin, A.A. Ruchika, M. Sen, T.Y. Sheikh-Jabbari, Is there an early universe solution to hubble tension? Phys. Rev. D **102**(10), 103525 (2020)
123. M.G. Dainotti, G. Sarracino, S. Capozziello, Gamma-ray bursts, supernovae ia, and baryon acoustic oscillations: A binned cosmological analysis. Publ. Astron. Soc. Jpn. **74**(5), 1095–1113 (2022)
124. G. Bargiacchi, M.G. Dainotti, S. Capozziello, High-redshift cosmology by Gamma-Ray Bursts: an overview. New Astron. Rev. **100**, 101712 (2025)
125. G. Risaliti, E. Lusso, Cosmological constraints from the hubble diagram of quasars at high redshifts. Nat. Astron. **3**(3), 272–277 (2019)
126. E. Lusso, G. Risaliti, E. Nardini, G. Bargiacchi, M. Benetti, S. Bisogni, S. Capozziello, F. Civano, L. Eggleston, M. Elvis et al., Quasars as standard candles-iii. validation of a new sample for cosmological studies. Astron. Astrophys. **642**, A150 (2020)
127. M.G. Dainotti, G. Bargiacchi, A.Ł Lenart, S. Nagataki, S. Capozziello, Quasars: Standard candles up to z= 7.5 with the precision of supernovae ia. Astrophys. J. **950**(1), 45 (2023)
128. M.G. Dainotti, G. Bargiacchi, A.Ł Lenart, S. Capozziello, E.Ó. Colgáin, R. Solomon, D. Stojkovic, M. Sheikh-Jabbari, Quasar standardization: overcoming selection biases and redshift evolution. Astrophys. J. **931**(2), 106 (2022)
129. G. Bargiacchi, M. Dainotti, S. Nagataki, S. Capozziello, Gamma-ray bursts, quasars, baryonic acoustic oscillations, and supernovae ia: new statistical insights and cosmological constraints. Mon. Not. R. Astron. Soc. **521**(3), 3909–3924 (2023)
130. S. Pourojaghi, N. Zabihi, M. Malekjani, Can high-redshift hubble diagrams rule out the standard model of cosmology in the context of cosmography? Phys. Rev. D **106**(12), 123523 (2022)
131. K.C. Wong, S.H. Suyu, G.C. Chen, C.E. Rusu, M. Millon, D. Sluse, V. Bonvin, C.D. Fassnacht, S. Taubenberger, M.W. Auger et al., H0licow-xiii. a 2.4 per cent measurement of h 0 from lensed quasars: 5.3 σ tension between early-and late-universe probes. Mon. Not. R. Astron. Soc. **498**(1), 1420–1439 (2020)
132. A.J. Shajib, S. Birrer, T. Treu, A. Agnello, E. Buckley-Geer, J. Chan, L. Christensen, C. Lemon, H. Lin, M. Millon et al., Strides: a 3.9 per cent measurement of the hubble constant from the strong lens system des j0408–5354. Mon. Not. R. Astron. Soc. **494**(4), 6072–6102 (2020)
133. M. Millon, A. Galan, F. Courbin, T. Treu, S. Suyu, X. Ding, S. Birrer, G.-F. Chen, A. Shajib, D. Sluse et al., Tdcosmo-i. an exploration of systematic uncertainties in the inference of h0 from time-delay cosmography. Astron. Astrophys. **639**, A101 (2020)
134. P. L. Kelly, S. Rodney, T. Treu, M. Oguri, W. Chen, A. Zitrin, S. Birrer, V. Bonvin, L. Dessart, J. M. Diego, et al., Constraints on the hubble constant from supernova refsdal's reappearance, Science 380 (6649), eabh1322 (2023)
135. M. Pascale, B.L. Frye, J.D. Pierel, W. Chen, P.L. Kelly, S.H. Cohen, R.A. Windhorst, A.G. Riess, P.S. Kamieneski, J.M. Diego et al., Sn h0pe: the first measurement of h0 from a multiply imaged type ia supernova, discovered by jwst. Astrophys. J. **979**(1), 13 (2025)
136. A.G. Riess, L. Macri, S. Casertano, H. Lampeitl, H.C. Ferguson, A.V. Filippenko, S.W. Jha, W. Li, R. Chornock, A 3% solution: determination of the hubble constant with the hubble space telescope and wide field camera 3. Astrophys. J. **730**(2), 119 (2011)
137. A.G. Riess, W. Yuan, L.M. Macri, D. Scolnic, D. Brout, S. Casertano, D.O. Jones, Y. Murakami, G.S. Anand, L. Breuval et al., A comprehensive measurement of the local value of the hubble constant with 1 $\mathrm{km} s^{-1}\ \mathrm{mpc}^{-1}$ uncertainty from the hubble space telescope and the sh0es team. The Astrophysical journal letters **934**(1), L7 (2022)
138. B.-H. Lee, W. Lee, E.Ó. Colgáin, M. Sheikh-Jabbari, S. Thakur, Is local h_0 at odds with dark energy eft? J. Cosmol. Astropart. Phys. **2022**(04), 004 (2022)
139. Y. Cai, X. Ren, T. Qiu, M. Li, X. Zhang, The Quintom theory of dark energy after DESI DR2, Natl Sci Rev. nwag115 (2026)
140. G. Ye, M. Martinelli, B. Hu, A. Silvestri, Hints of nonminimally coupled gravity in desi 2024 baryon acoustic oscillation measurements. Phys. Rev. Lett. **134**(18), 181002 (2025)
141. G. Gu et al., Dynamical dark energy in light of the DESI DR2 baryonic acoustic oscillations measurements. Nature Astron. **9**(12), 1879–1889 (2025)
142. G. Efstathiou, S. Gratton, A Detailed Description of the CAMSPEC Likelihood Pipeline and a Reanalysis of the Planck High Frequency Maps, Open J. Astrophys. 4 (2021)
143. E. Rosenberg, S. Gratton, G. Efstathiou, Cmb power spectra and cosmological parameters from planck pr4 with camspec. Mon. Not. R. Astron. Soc. **517**(3), 4620–4636 (2022)
144. J. Carron, M. Mirmelstein, A. Lewis, Cmb lensing from planck pr4 maps. J. Cosmol. Astropart. Phys. **2022**(09), 039 (2022)
145. M.S. Madhavacheril, F.J. Qu, B.D. Sherwin, N. MacCrann, Y. Li, I. Abril-Cabezas, P.A. Ade, S. Aiola, T. Alford, M. Amiri et al., The atacama cosmology telescope: Dr6 gravitational lensing map and cosmological parameters. Astrophys. J. **962**(2), 113 (2024)
146. J. Carron, A. Lewis, G. Fabbian, Planck integrated sachs-wolfe-lensing likelihood and the cmb temperature. Phys. Rev. D **106**(10), 103507 (2022)
147. F.J. Qu, B.D. Sherwin, M.S. Madhavacheril, D. Han, K.T. Crowley, I. Abril-Cabezas, P.A. Ade, S. Aiola, T. Alford, M. Amiri et al., The atacama cosmology telescope: A measurement of the dr6 cmb lensing power spectrum and its implications for structure growth. Astrophys. J. **962**(2), 112 (2024)
148. T.-N. Li, G.-H. Du, S.-H. Zhou, Y.-H. Li, J.-F. Zhang, X. Zhang, Robust evidence for dynamical dark energy in light of DESI DR2 and joint ACT, SPT, and Planck data. Phys. Dark Univ. **52**, 102254 (2026)
149. T. Louis, A. La Posta, Z. Atkins, H.T. Jense, I. Abril-Cabezas, G.E. Addison, P.A. Ade, S. Aiola, T. Alford, D. Alonso et al., The atacama cosmology telescope: Dr6 power spectra, likelihoods and λcdm parameters. J. Cosmol. Astropart. Phys. **2025**(11), 062 (2025)
150. W. Quan, SPT-3G D1: Maps of the millimeter-wave sky from 2019 and 2020 observations of the SPT-3G Main field. arXiv:2603.20163 (2026)

151. E. Özülker, E.D. Valentino, W. Giarè, Dark energy crosses the line: Quantifying and testing the evidence for phantom crossing. arXiv:2506.19053 (2025)
152. R. Chen, J.M. Cline, V. Muralidharan, B. Salewicz, Quintessential dark energy crossing the phantom divide. JCAP **03**, 044 (2026)
153. E. Silva, R.C. Nunes, Testing signatures of phantom crossing through full-shape galaxy clustering analysis. JCAP **11**, 078 (2025)
154. N. Roy, S. Chakrabarti, Is phantom barrier crossing inevitable? a cosmographic analysis. arXiv:2508.13740 (2025)
155. S.L. Guedezounme, B.R. Dinda, R. Maartens, Phantom crossing or dark interaction? JCAP **01**, 062 (2026)
156. W. Hu, Crossing the phantom divide: dDark energy internal degrees of freedom. Phys. Rev. D-Particles Fields Gravitation Cosmol. **71**(4), 047301 (2005)
157. Z. Yao, G. Ye, A. Silvestri, A general model for dark energy crossing the phantom divide. J. Cosmol. Astropart. Phys. **2025**(10), 078 (2025)
158. Y.-F. Cai, E.N. Saridakis, M.R. Setare, J.-Q. Xia, Quintom Cosmology: theoretical implications and observations. Phys. Rept. **493**, 1–60 (2010)
159. T. Qiu, Theoretical Aspects of Quintom Models. Mod. Phys. Lett. A **25**, 909–921 (2010)
160. A. Vikman, Can dark energy evolve to the phantom? Phys. Rev. D **71**, 023515 (2005)
161. C. Deffayet, O. Pujolas, I. Sawicki, A. Vikman, Imperfect Dark Energy from Kinetic Gravity Braiding. JCAP **10**, 026 (2010)
162. W.J. Wolf, P.G. Ferreira, Underdetermination of dark energy. Phys. Rev. D **108**(10), 103519 (2023)
163. D. Shlivko, P.J. Steinhardt, Assessing observational constraints on dark energy. Phys. Lett. B **855**, 138826 (2024)
164. W.J. Wolf, C. García-García, D.J. Bartlett, P.G. Ferreira, Scant evidence for thawing quintessence. Phys. Rev. D **110**(8), 083528 (2024)
165. M. Cortês, A.R. Liddle, Interpreting DESI's evidence for evolving dark energy. JCAP **12**, 007 (2024)